Received: 26 February 2024 | Revised: 11 June 2024 | Accepted: 16 June 2024

DOI: 10.1002/pro.5094

RESEARCH ARTICLE

THE PROTEIN SOCIETY WILEY

Elaboration of the Homer1 recognition landscape reveals incomplete divergence of paralogous EVH1 domains

Avinoam Singer[1] | **Alejandra Ramos**[1] | **Amy E. Keating**[1,2,3]

[1]Department of Biology, Massachusetts Institute of Technology, Cambridge, Massachusetts, USA

[2]Department of Biological Engineering, Massachusetts Institute of Technology, Cambridge, Massachusetts, USA

[3]Koch Institute for Integrative Cancer Research, Massachusetts Institute of Technology, Cambridge, Massachusetts, USA

Correspondence
Amy E. Keating, Department of Biology, Massachusetts Institute of Technology, 77 Massachusetts Ave., Cambridge, MA 02139, USA.
Email: keating@mit.edu

Funding information
National Institutes of Health, Grant/Award Numbers: R01 GM129007, R35 GM149227; National Cancer Institute, Grant/Award Number: P30-CA14051; National Institute of General Medical Sciences, Grant/Award Number: T32 GM007287

Review Editor: John Kuriyan

Abstract

Short sequences that mediate interactions with modular binding domains are ubiquitous throughout eukaryotic proteomes. Networks of short linear motifs (SLiMs) and their corresponding binding domains orchestrate many cellular processes, and the low mutational barrier to evolving novel interactions provides a way for biological systems to rapidly sample selectable phenotypes. Mapping SLiM binding specificity and the rules that govern SLiM evolution is fundamental to uncovering the pathways regulated by these networks and developing the tools to manipulate them. We used high-throughput screening of the human proteome to identify sequences that bind to the Enabled/VASP homology 1 (EVH1) domain of the postsynaptic density scaffolding protein Homer1. This expanded our understanding of the determinants of Homer EVH1 binding preferences and defined a new motif that can facilitate the discovery of additional Homer-mediated interactions. Interestingly, the Homer1 EVH1 domain preferentially binds to sequences containing an N-terminally overlapping motif that is bound by the paralogous family of Ena/VASP actin polymerases, and many of these sequences can bind to EVH1 domains from both protein families. We provide evidence from orthologous EVH1 domains in pre-metazoan organisms that the overlap in human Ena/VASP and Homer binding preferences corresponds to an incomplete divergence from a common Ena/VASP ancestor. Given this overlap in binding profiles, promiscuous sequences that can be recognized by both families either achieve specificity through extrinsic regulatory strategies or may provide functional benefits via multi-specificity. This may explain why these paralogs incompletely diverged despite the accessibility of further diverged isoforms.

KEYWORDS
binding specificity, Ena/VASP, EVH1, Homer, peptide library, protein evolution, short linear motif

1 | INTRODUCTION

Biological systems encode numerous modular interaction domains that have expanded into families of paralogs (Bhattacharyya et al., 2006). Many of these domains recognize stretches of 3–10 sequential residues within intrinsically disordered regions, termed short linear motifs (SLiMs) (Tompa et al., 2014). Compared to interactions between globular domains, SLiM-mediated interactions are typically weak ($K_D > 10$ μM) and transient, making them ideal for dynamic processes such as signaling (Wright and Dyson, 2015). SLiMs are also used for protein localization and to coordinate molecular assemblies (Van Roey et al., 2014).

SLiM binding domains (SBDs) have characteristic motif preferences that are often described using regular expressions that indicate invariant or common residues found in known interaction partners. Matches to these low-information expressions are prevalent throughout the proteome, suggesting that these short sequences alone are poor predictors of binding. Indeed, high-throughput screens of peptide libraries have shown that although most sequences that bind to a given domain share features of a defining motif, not every sequence that matches that motif will bind. Many case studies illustrate how residues outside the core motif can modulate both the affinity and specificity of binding, demonstrating that motifs provide only a partial picture of domain-SLiM molecular recognition (Bugge et al., 2020; Foight and Keating, 2016). For example, higher affinity SLiM-mediated interactions, with K_D <1 μM, often form additional domain contacts using residues flanking the SLiM (Hwang et al., 2021; Li et al., 2018).

Nature has harnessed SLiM interaction networks to build increasingly complex systems, as evidenced by the rapid expansion of SBD families in higher eukaryotes (Vogel and Chothia, 2006). As SBD modules are duplicated, paralogous domains must distinguish their networks to minimize competitive interference and support new functions (Conant and Wolfe, 2008; Davey et al., 2015). Distinct interaction niches can be established in a manner that is extrinsic to the properties of the SBD domain itself, through means such as spatiotemporal compartmentalization of protein expression. Alternatively, this can be achieved intrinsically, at the level of molecular recognition, through sequence changes that alter SBD interaction specificity (Davey et al., 2012).

The dual promise of unraveling SLiM-mediated networks to uncover novel biology and rewiring such networks to build pathways, for example, for applications in synthetic biology or as molecular therapies, necessitates a clear understanding of how specificity is established. Here, we explore this question by investigating the divergence of Enabled/VASP homology 1 (EVH1) domains. The human genome encodes 5 EVH1-containing protein families: WASP, SPRED, PP4, Ena/VASP, and Homer (Peterson and Volkman, 2009; Ueki et al., 2019). Ena/VASP and Homer are thought to have diverged from a common ancestor, and distinct Ena/VASP and Homer proteins in the choanoflagellate *Salpingoeca rosetta* suggest that this event occurred at least 600 million years ago (Ayala et al., 1998; Burkhardt et al., 2014).

The Ena/VASP family encompasses three members: ENAH, VASP, and EVL (Faix and Rottner, 2022). These tetrameric proteins regulate the actin cytoskeleton by serving as a scaffold and acting as processive actin polymerases (Bachmann et al., 1999; Bear and Gertler, 2009; Hüttelmaier et al., 1999). Ena/VASP EVH1 domains localize these proteins to sites of actin polymerization, such as filopodia, lamellipodia, and neuronal projections (Drees and Gertler, 2008; Lanier et al., 1999; Reinhard et al., 1995; Rottner et al., 1999).

Like Ena/VASP, the Homer family contains three members: Homer1, Homer2, and Homer3 (Shiraishi-Yamaguchi and Furuichi, 2007). The constitutively expressed tetrameric Homer proteins function as scaffolds within the post-synaptic density of neurons (Tu et al., 1998, 1999). Alternatively spliced, monomeric Homer isoforms dynamically regulate signaling pathways by competing with tetrameric Homer and disassembling these complexes in response to neuronal activity (Clifton et al., 2019; Xiao et al., 1998). In this capacity, Homer contributes to synaptic plasticity by regulating dendritic spine morphology, perhaps through direct association with actin cytoskeleton proteins such as the actin-binding protein DBN1 (Brakeman et al., 1997; Li et al., 2019). Homer proteins are also expressed in a variety of non-neuronal tissues (Xiao et al., 1998). For example, Homer3 negatively regulates T-cell activation by competing with calcineurin for binding to NFATc2 (Huang et al., 2008).

Sequences of known Ena/VASP partners have revealed the interaction motif [FWYL]PxΦP (Φ = FWYPIALV; x = any amino acid) (Dinkel et al., 2012; Niebuhr et al., 1997). Several studies have also demonstrated strategies by which regions flanking the core Ena/VASP motif can modulate both affinity and specificity for the EVH1 domain (Acevedo et al., 2017; Hwang et al., 2022; Niebuhr et al., 1997). Fewer Homer binding partners have been validated, and the sequence preferences are less well-defined. Alignments of Homer binding partners suggest a consensus sequence of PPxxF; peripheral regions that modulate the affinity of this motif are poorly understood (Dinkel et al., 2012; Tu et al., 1998). Structural alignments of the homologous EVH1 domains in complex with their ligands show that Ena/VASP and Homer families of proteins use partially overlapping binding sites

to engage their proline-rich ligands (Beneken et al., 2000; Prehoda et al., 1999).

In this study, we applied high-throughput screening of a library derived from the human proteome to identify Homer1 binding peptides. We found that Homer1 binds to a more general motif than PPxxF and demonstrated how residues flanking the core motif can tune the affinity of this interaction. Notably, compared to the PPxxF motif alone, Homer1 EVH1 domain binds with enhanced affinity to many short segments in the human proteome that match both the Ena/VASP and Homer binding motifs, despite lacking structural features thought to confer these preferences in Ena/VASP proteins. Specifically, we demonstrate that many peptides that contain an N-terminal, overlapping Ena/VASP motif bind with increased affinity to Homer1 while retaining the ability to bind to ENAH. An examination of orthologous EVH1 domains in pre-metazoan organisms suggests that this Homer preference is a vestige of EVH1 domains found in organisms that predate the duplication event that gave rise to distinct Ena/VASP and Homer protein families.

2 | RESULTS

2.1 | Structural comparison of related EVH1 domains

Despite only sharing 30% overall sequence identity, the Ena/VASP and Homer EVH1 domain binding sites exhibit a high degree of structural similarity (Figure 1a). Each site is comprised of a proline-binding groove and a neighboring pocket that accommodates an N- or C-terminal core-motif hydrophobic residue (Figure 1b) (Beneken et al., 2000; Prehoda et al., 1999).

Within the proline-binding grooves of Ena/VASP and Homer, aromatic residues ($W23_{ENAH}$, $F77_{ENAH}$, $Y16_{ENAH}$; $W24_{Homer1}$, $F74_{Homer1}$, $F14_{Homer1}$) accommodate the distinct polyproline-II helical structure adopted by the proline tracts of bound peptides. We use a unified numbering scheme in this work, defined in Figure 1, in which the Ena/VASP and Homer motifs are indicated as $^{-3}$[FWYL]PxΦP^{1} and ^{0}PPxxF^{4}, respectively. The positioning of aromatic residues within the EVH1 domain groove differs between the two families and is thought to define the locations of required prolines within each preferred motif (Conant and Wolfe, 2008). For example, the unique Ena/VASP aromatic residue, $Y16_{ENAH}$ ($I16_{Homer1}$) engages Pro^{-2}, and a preference for Pro at this position is absent from the Homer motif. Conversely, the unique Homer aromatic residue, $F14_{Homer1}$ ($M14_{ENAH}$) engages Pro^{1}. Both families conserve aromatic residues at positions 23 (ENAH)/24 (Homer1) and 77 (ENAH)/77 (Homer1), which engage motif residues Pro^{-2} and Pro^{1}.

The peptide-binding specificity of each domain arises from distinct hydrophobic pockets on opposite ends of the proline-binding groove. The Ena/VASP pocket, which we designate here as P_{EV}, is primarily formed by $K69_{ENAH}$ ($T66_{Homer1}$), $N71_{ENAH}$ ($T68_{Homer1}$), and $R81_{ENAH}$ ($A78_{Homer1}$), which can form a cation-pi

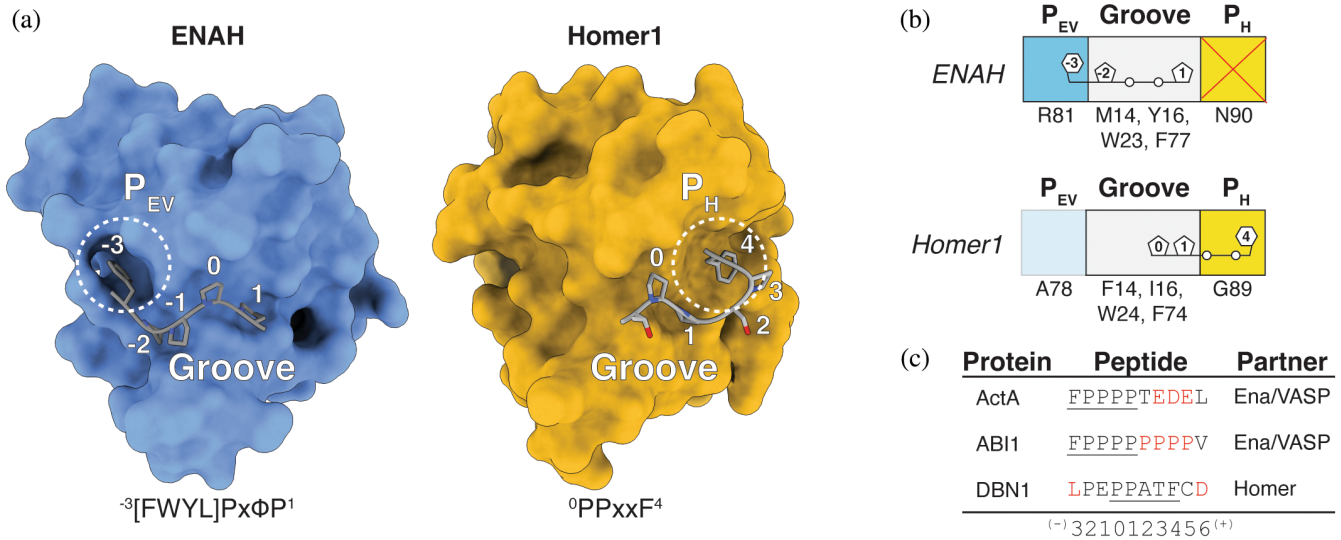

FIGURE 1 (a) Structures of ENAH (1EVH) and Homer1 (1DDV) in complex with representative ligands. Peptide numbering is relative to the Homer PPxxF motif. For Ena/VASP motifs, the numbering defines the proline that is common to both motifs as position 1 (Beneken et al., 2000; Prehoda et al., 1999). (b) Cartoon representation of the modular binding pockets along the Ena/VASP and Homer EVH1 domains. (c) Flanking residues (red) that are reported to enhance the affinity of a motif (underlined) for Ena/VASP and Homer EVH1 domains (Hwang et al., 2022; Li et al., 2019; Niebuhr et al., 1997).

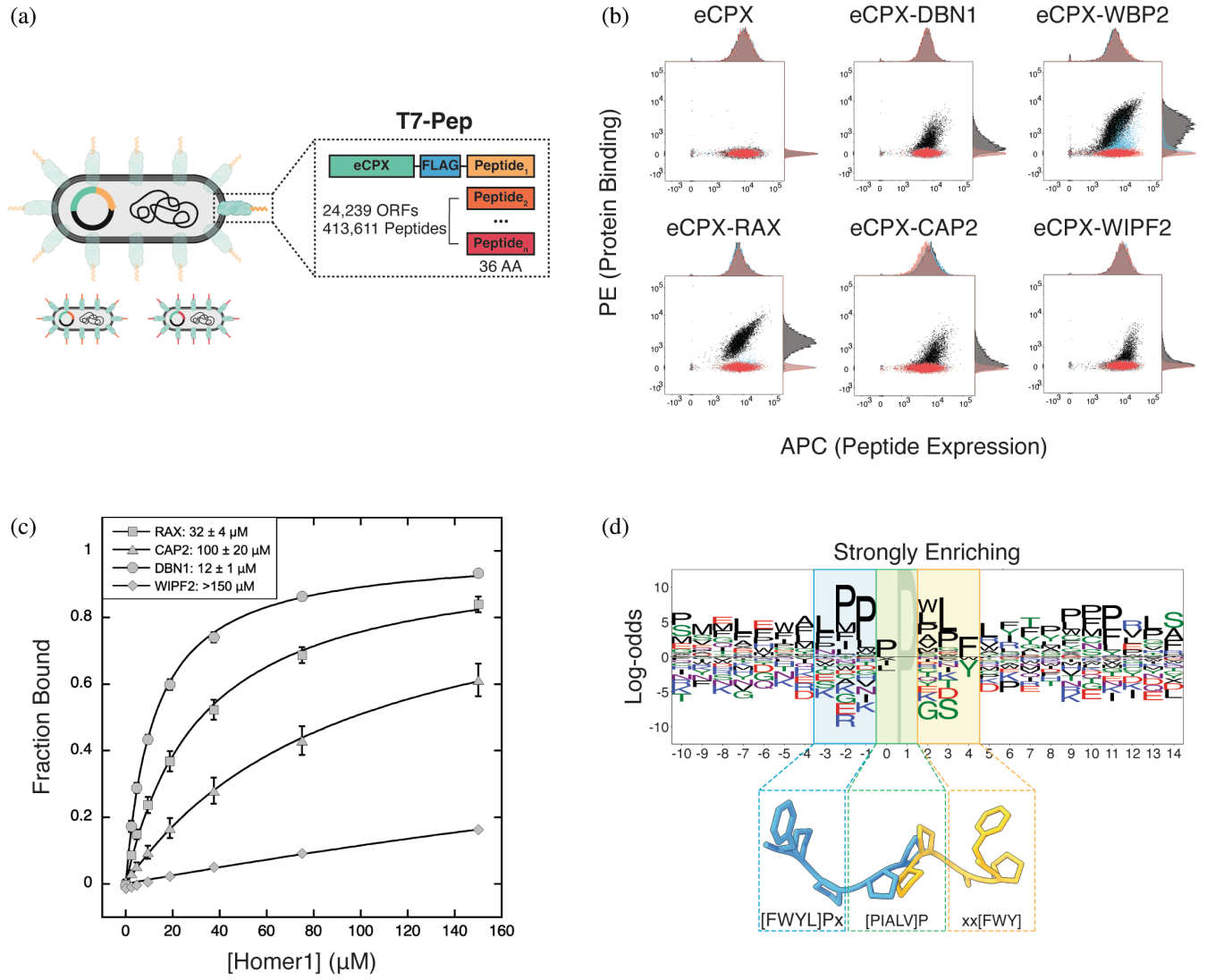

FIGURE 2 (a) The T7-pep library encodes 36-residue fragments of the human proteome as C-terminal extensions of the *Escherichia coli* surface protein eCPX. (b) Single-clone surface display measurements of control (eCPX, DBN1) and T7-pep derived peptides (from WBP2, RAX, CAP2, WIPF2) against Homer1 EVH1 domain tetramers (black) and binding site mutants (red = Homer1^{W24A}, blue = Homer1^{G89N}). (c) BLI measurements and binding affinities of control (DBN1) and T7-pep derived peptides (from RAX, CAP2, WIPF2) binding to Homer1 EVH1 domain monomer. (d) Sequence logo of peptides strongly enriched for Homer1 EVH1 binding, aligned by their motifs. Below the logo is a superposition of peptides as they bind to ENAH (blue) or Homer1 (yellow) EVH1 domains. The EVH1 domains in structures 1EVH and 1DDV were superimposed and then the domains were deleted (Beneken et al., 2000; Prehoda et al., 1999). The logo and structural representation illustrate the similarity between the Homer1 N-terminal motif flank and the Ena/VASP motif (blue = Ena/VASP-like flank, green = overlapping prolines, yellow = Homer-specific motif residues) (Beneken et al., 2000; Prehoda et al., 1999). Peptide sequences for (b) and (c) are given in Table 1. BLI, biolayer interferometry.

interaction when the residue N-terminal to the motif prolines is aromatic ($^{-3}$**[FWYL]**PxΦP^{1}). Although the Homer EVH1 domain lacks a well-formed P_{EV}, residues in this region do not sterically occlude this pocket. The Homer pocket, which we call P_H, lies at the other end of the proline-binding groove and is formed by $G89_{Homer1}$. P_H can accommodate Phe at position 4 (^{0}PPxx**F**^{4}), whereas in Ena/VASP proteins, this pocket is obstructed by the corresponding $N90_{ENAH}$.

In addition to the core motif, residues in the surrounding sequence can contribute to the affinity and specificity of a peptide for an SBD (Figure 1c) (Bugge et al., 2020). Several affinity-enhancing elements have been discovered for Ena/VASP domains. Acidic residues flanking the $^{-3}$[FWYL]PxΦP^{1} motif strengthen binding to positively charged patches along the domain (Niebuhr et al., 1997). C-terminal proline extensions, such as in a peptide from ABI1 ($^{-3}$FPPPP**PPP**^{4}), position the motif-

TABLE 1 T7-pep derived and control (DBN1) peptides that bound to Homer1 via bacterial surface display.

Protein name	Peptide sequence
DBN1	LNFDELPE**PPATF**CDPEEVE
WBP2	**PPPEF**YPGPPMMDGAMGYVQP**PPPPY**PGPMEPPVSG
RAX	GFGPPAQSLPASYTPPP**PPPPF**LNSPPLGPGLQPLA
CAP2	KSSEMNILIPQDGDYREFP**IPEQF**KTAWDGSKLITE
WIPF2	VEDFP**APEEY**KHFQRIYPSKTNRAARGAPPLPPILR

Note: Sites matching the expanded Homer1 EVH1 domain binding motif ^{0}[PIALV]Pxx[FWY]^{4} are marked in bold.

trailing residues so they can make favorable hydrophobic contacts near the region corresponding to Homer P_H (Hwang et al., 2022). Finally, Ena/VASP EVH1 domains have been shown to bind a secondary motif at a pseudo-symmetric binding site on the opposite face of the domain (FPPPx$_n$**FPPPP**) (Acevedo et al., 2017; Hwang et al., 2022). Few flanking elements have been uncovered for Homer EVH1 domains, although examinations of a handful of known Homer binding partners and mutational studies of a SLiM from the protein DBN1 indicate that Homer prefers an N-terminal Leu (**L**(x)$_{1\text{-}2}$PPxxF^{4}) and a C-terminal Asp/Asn (^{0}PPxxFx**[DN]**) (Li et al., 2019).

2.2 | A proteome-wide screen elaborates the Homer1 binding motif

High-throughput screening of peptide libraries can reveal molecular determinants of SBD interactions (Davey et al., 2017). The T7-pep library encodes the human proteome as 416,611 36-mer peptides and provides a biologically relevant context for identifying putative SBD binding preferences and native interaction partners (Figure 2a) (Larman et al., 2011). Hwang et al. formatted this library for bacterial surface display at the C-terminus of the *Escherichia coli* surface protein eCPX and used screening to identify elements that flank the Ena/VASP motif and modulate binding to ENAH (Hwang et al., 2022; Rice and Daugherty, 2008).

We performed an enrichment screen of the T7-pep library to identify Homer1 EVH1 domain binding peptides. To assess the success of the screen, we initially sequenced a set of individual clones from different rounds of enrichment. Reassuringly, this initial analysis revealed sequences containing the previously identified PPxxF motif, including peptides from the metabotropic glutamate receptor GRM5, a well-established Homer interaction partner, and WBP2, a protein that binds to Homer3 (Table 1) (Chen et al., 2018; Tu et al., 1998). We also discovered matches to this motif in screening hits not yet annotated as Homer binding partners, such as the protein RAX, which regulates retinal and neural development (Muranishi et al., 2012). For several peptides (Table 1), we verified binding to Homer1 EVH1 domain tetramers, using the cell-surface display assay, and quantified binding to the monomeric EVH1 domain using biolayer interferometry (BLI) (Figure 2b,c).

Our initial small-scale sequencing identified several clones that deviated from the published PPxxF motif by substitution of a small hydrophobic residue at Pro^{0} or substitution of Trp or Tyr at Phe^{4} (Table 1). Testing bacterial clones displaying peptides from the proteins WIPF2 (APEEY) and CAP2 (IPEQF) confirmed binding to Homer1 EVH1, and these peptides did not bind detectably to variants of the EVH1 domain with a disrupted proline binding groove (Homer1^{W24A}) or with an occluded P_H pocket (Homer1^{G89N}), suggesting a shared binding mode with the canonical motif (Figure 2b) (Beneken et al., 2000). BLI measurements showed that these peptides that do not match the consensus motif bound with lower affinity than those including PPxxF sequences (Figure 2b, Table 2). Based on these experiments, we relaxed our definition of the Homer1 EVH1 domain binding motif to ^{0}[PIALV]Pxx[FWY]^{4}.

Having established that the screen successfully isolated valid Homer1 EVH1 binders, we used deep sequencing and enrichment analysis to identify 360 weakly enriching and 62 strongly enriching peptides that matched the expanded motif ^{0}[PIALV]Pxx[FWY]^{4} (Figure S1A in Data S1, Table S1). Among these, we identified peptides that bound with affinities ranging from 15 to 100 μM, by BLI, which is within the range of affinities of established Homer binding sequences (Table 2). Interestingly, a peptide from the protein PSORS1C2, which lacks a canonical motif but contains the sequence APPLF, bound with $K_D = 15 \pm 1$ μM, similar to the affinity of peptides containing the canonical motif.

2.3 | An N-terminal Ena/VASP motif enhances Homer1 binding

Approximately 97% of sequences matching the ^{0}[PIALV]Pxx[FWY]^{4} motif that were present in the T7-pep library

TABLE 2 Binding affinities of peptides from the T7-pep enrichment screen and DVL3 peptide point mutants for Homer1 EVH1 domain, measured by BLI.

Protein name	Peptide sequence	K_D (μM)
SMR3B	YPPGPLA**PPQPF**GPGFVPPP**PPPPY**GPGRIPPPPPA	15 ± 1
PSORS1C2	PPAEDREEAGSPTLPQGPPVPGDPWPG**APPLF**EDPP	15 ± 1
HOXB2	ETFQTSSIKESTLIP**PPPPF**EQTFPSLQPGASTLQR	17 ± 1
WASF2	FSEDNLPP**PPAEF**SYPVDNQRGSGLAGPKRSSVVSP	18 ± 1
RAX	GFGPPAQSLPASYTPPP**PPPPF**LNSPPLGPGLQPLA	32 ± 4
GRID2IP	PLSPPPP**PPLPF**HDAKPSSRSSDGSRGPAQALAKRL	61 ± 7
LSR	SEERRRPHKEEEEEAYYPP**APPPY**SETDSQASRERR	62 ± 2
CAP2	KSSEMNILIPQDGDYREFP**IPEQF**KTAWDGSKLITE	100 ± 20
NEDD4L	EVVDSNDSASQHQEELPPPP**LPPGW**EEKVDNLGRTY	100 ± 3
SH2B1	MNGAPSPEDGASPSSPPLPPP**PPPSW**REFCESHARP	113 ± 6
WIPF2	VEDFP**APEEY**KHFQRIYPSKTNRAARGAPPLPPILR	>150
GPR179	MGTRGAVM**PPPMW**GLLGCCFVCAWALGGPRPIRSLP	>150
ROCK2	ADAKE**IPRIF**QILYANEGESKKEQEFPVEPVGEKSN	>150
NFASC	MARQ**PPPPW**VHAAFLLCLLSLGGAIEIPMDPSIQNE	>150
DVL3	PLPHPGAAPWPMAFPYQYPP**PPHPY**NPHPGFPELGY	46 ± 6
$DVL3^{Y(-3)A}$	PLPHPGAAPWPMAFPYQAPP**PPHPY**NPHPGFPELGY	104 ± 8
$DVL3^{P(-2)A}$	PLPHPGAAPWPMAFPYQYAP**PPHPY**NPHPGFPELGY	145 ± 20
$DVL3^{P(-1)A}$	PLPHPGAAPWPMAFPYQYPA**PPHPY**NPHPGFPELGY	80 ± 20
$DVL3^{P0A}$	PLPHPGAAPWPMAFPYQYPP**APHPY**NPHPGFPELGY	115 ± 10
$DVL3^{P1A}$	PLPHPGAAPWPMAFPYQYPP**PAHPY**NPHPGFPELGY	>150
$DVL3^{Y4F}$	PLPHPGAAPWPMAFPYQYPP**PPHPF**NPHPGFPELGY	14 ± 1
$DVL3^{Y4W}$	PLPHPGAAPWPMAFPYQYPP**PPHPW**NPHPGFPELGY	51 ± 4
$DVL3^{Y4A}$	PLPHPGAAPWPMAFPYQYPP**PPHPA**NPHPGFPELGY	>150

Note: Matches to the expanded Homer1 binding motif are shown in bold. Values represent the average and standard deviation of three replicates.

failed to enrich, even in the avid conditions of the screen, which used a tetramerized Homer1 EVH1 domain. To uncover elements that modulate motif affinity for Homer1, we visualized the screen results using pLogo, which scales residue height according to over- and under-representation relative to background amino-acid frequencies (O'Shea et al., 2013). Weakly and strongly enriching sequences were aligned by their motifs and compared to a background of all Homer motif instances in the input library (Figure 2d, Figure S1B in Data S1).

Notably, the logo of strongly enriching sequences unveiled a preference for the residues $^{-3}$[LF]PP^{-1} immediately N-terminal to the Homer motif ($^{-3}$**[LF]PP**[PIALV]Pxx[FWY]^{4}). These residues resemble the Ena/VASP motif, often encountered as the sequence $^{-3}$[FWYL]PPPP^{1}. We refer to the motif $^{-3}$[LF]PP[PIALV]Pxx[FWY]^{4} as the extended Homer motif and the [LF]PP sequence as the Ena/VASP-like flank. Comparison of structures of Ena/VASP (PDB: 1EVH) versus Homer (PDB: 1DDV) EVH1 domains bound to motif-matching peptides shows that the two C-terminal prolines of the Ena/VASP motif ($^{-3}$[FWYL]PPPP^{1}) bind to Ena/VASP in a pose similar to how the first two prolines of the (^{0}PPSTF^{4}) motif bind to Homer (Figure 2d) (Beneken et al., 2000; Prehoda et al., 1999). This structural alignment predicts that the N-terminal flanking residues that are enriched in the sequence logo may dock with Homer1 in a manner similar to the binding of a canonical Ena/VASP ligand to Ena/VASP EVH1, despite the absence of a well-formed P_{EV} pocket or the residue $Y16_{ENAH}$ that is used by Ena/VASP proteins for Pro^{-2} docking.

Segment polarity protein disheveled homology DVL3, a key player in the Wnt signaling pathway, binds to Homer3 in a yeast two-hybrid assay (Luck et al., 2020). While DVL3 does not contain a canonical PPxxF motif, a peptide containing the noncanonical motif and an Ena/VASP-like N-terminal flank ($^{-3}$YPPPPHPY^{4}) enriched in our screen and bound with $K_D = 46 \pm 6$ μM. Alanine substitutions throughout this sequence were tolerated to varying degrees (Table 2). Within the core motif, the substitution of Pro^{1} or Tyr^{4} with Ala resulted

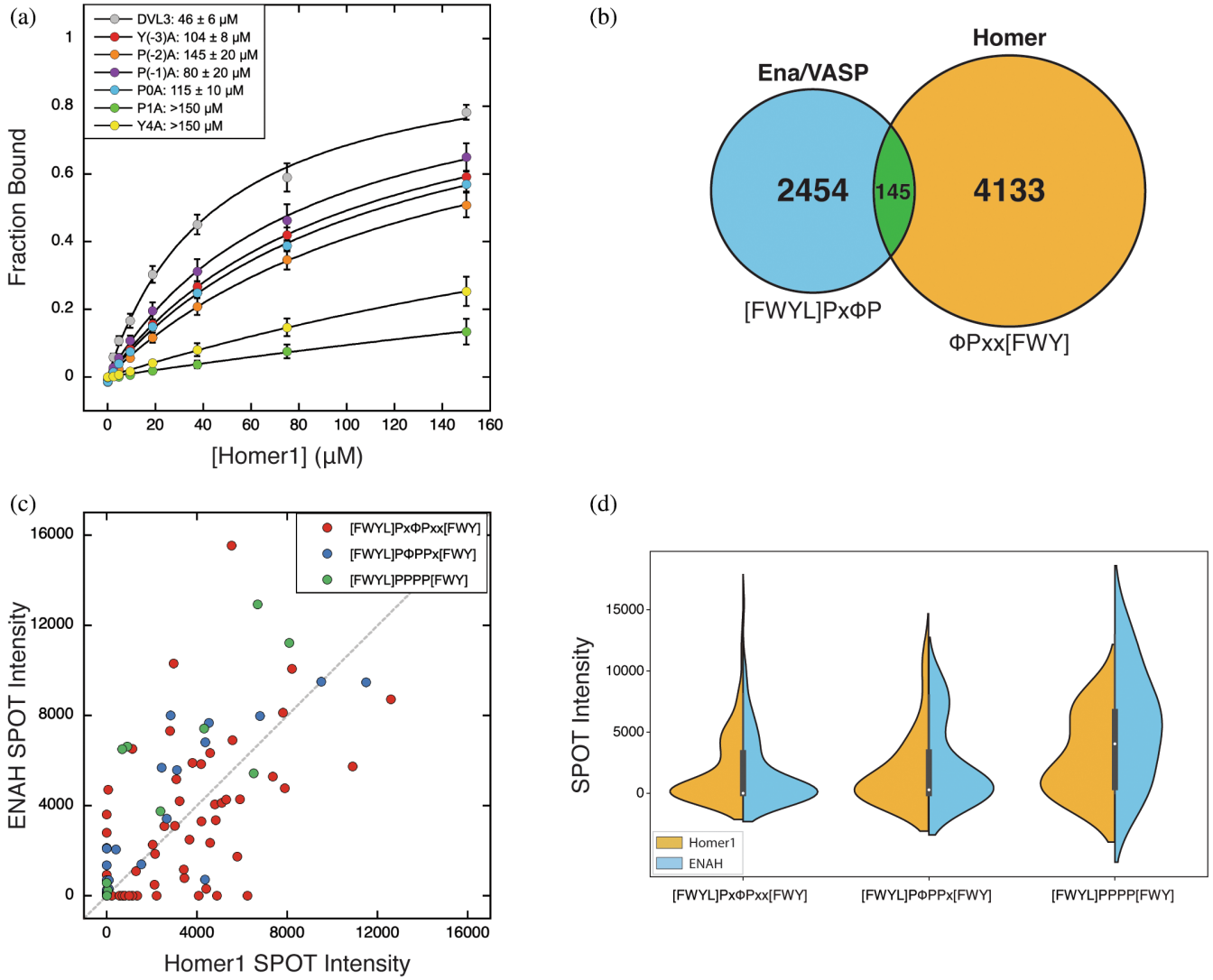

FIGURE 3 (a) Alanine mutations throughout the Homer1 motif and the N-terminal Ena/VASP-like flank in DVL3 diminish binding to Homer1 EVH1. Peptide sequences are in Table 2. (b) The number of peptides that match the Ena/VASP (blue), Homer (gold), and overlapping motifs (green; $^{-3}$[FWYL]PxΦPxx[FWY]^4, $^{-2}$[FWYL]PΦPPx[FWY]^4, or $^{-1}$[FWYL]PPPP[FWY]^4) within disordered regions of the human proteome. (c and d) SPOT array intensities for ENAH and Homer1 EVH1 domain tetramers binding to human peptides containing overlapping Ena/VASP and Homer motifs.

in peptides without appreciable binding to Homer1 EVH1, while substitutions of Pro^0 caused nearly a three-fold reduction in binding affinity (Figure 3a). Mutations within the Ena/VASP-like flank had a similar impact on overall binding affinity as substitution of Pro^0 or the aromatic residue at position 4, highlighting the extent to which motif-external elements can influence binding. Interestingly, most of the BLI-validated sequences contained at least a partial match to the Ena/VASP-like flank, which was absent from nonbinding sequences with noncanonical motifs. These results demonstrate that an Ena/VASP-like flank can enhance Homer1 binding and compensate for a suboptimal core Homer motif.

2.4 | The Homer1 and ENAH EVH1 domains have incompletely diverged

The identification of an N-terminal Ena/VASP motif as a Homer affinity-enhancing flanking element is perplexing. Homer proteins are highly expressed in neurons, where Ena/VASP proteins play important roles in neuronal migration and axon guidance (Drees and Gertler, 2008). If Ena/VASP EVH1 domains are similarly capable of binding these overlapping motifs, that would imply the potential for competitive binding between the two protein families that have different functions.

The intrinsically disordered regions of the human proteome (with IUPRed >0.45) contain 103 instances of a

TABLE 3 Binding affinities of bioinformatically identified peptides containing the extended Homer motif (bold) for Homer1 or ENAH EVH1 domains, determined using BLI.

Protein name	Peptide sequence	K_D^{ENAH} (μM)	K_D^{Homer1} (μM)
ABI3	GDELG**LPPPPPGF**GPDEPSW	26 ± 1	3.9 ± 0.1
ABI3^{G5P}	GDELG**LPPPPPGF**PPDEPSW	40 ± 6	140 ± 10
DBN1	LNFDE**LPEPPATF**CDPEEVE	57 ± 1	12 ± 1
DBN1^{C5P}	LNFDE**LPEPPATF**PDPEEVE	65 ± 6	>150
WASF2	FSEDN**LPPPPAEF**SYPVDNQ	17.9 ± 0.4	13 ± 1
APBB1IP (2)	LDDPE**LPPPPPDF**MEPPPDF	8.2 ± 0.1	25 ± 1*
WBP2	PPGYP**YPPPPPEF**YPGPPMM	12 ± 2*	17 ± 2*
CEBPB	PACLP**LPPPPPAF**KSMEVAN	57 ± 9	37 ± 4
IQSEC3	THQPP**LPPPPPPY**NHPHQFC	57 ± 6	38 ± 4
FAT1	DIESD**FPPPPEDF**PAADELP	13.7 ± 0.3	98 ± 7
FAT1^{P5G}	DIESD**FPPPPEDF**GAADELP	17 ± 1	15 ± 1
ABB1IP (1)	TGGGG**LPAPPDDF**LPPPPPP	26 ± 1*	>150
PCDH15	PPSIP**LPLPPPTF**FPLSVST	108 ± 28	>150
DSCAM	GTLQI**FPFPPSSF**STLIHDN	>150	55 ± 4
RARA	GHLNG**YPVPPYAF**FFPPMLG	>150	100 ± 20
PRRC2B	HVDSV**LPVPPIEF**GVSPKDS	>150	100 ± 20
KANK4	PNHLP**LPGPPFSF**QNVLVVL	>150	>150
FLNC	FIAHI**LPAPPDCF**PDKVKAF	>150	>150
SH3BGRL	RPATG**YPLPPQIF**NESQYRG	>150	>150
DVL1	GYPYQ**YPGPPPCF**PPAYQDP	>150	>150

Note: Measurements marked with an asterisk (*) are peptides for which SPOT array binding was maintained even when the motif was disrupted via the mutation of the underlined residues to glycine. Values represent the average and standard deviation of three replicates.

Homer motif flanked by a potentially affinity-enhancing Ena/-VASP-like sequence, $^{-3}$**[FWYL]PxΦ**Pxx[FWY]^4 (Figure 3b, Table S2) (Mészáros et al., 2018). To determine whether peptides that match the core motifs of both domains bind to both Ena/VASP and Homer EVH1 domains, we tested the interaction of these peptides with tetrameric EVH1 constructs using a peptide SPOT array, in which peptides are synthesized on a nitrocellulose membrane (Figure 3c, Figure S2 in Data S1). Peptide arrays do not provide quantitative measures of binding affinity but can be used to identify binding regions and to qualitatively assess the effects of mutations (Ball et al., 2000, 2005). Many of the arrayed peptides bound to both domains and the distributions of intensities for all peptides were remarkably similar for Homer1 and ENAH EVH1 domains (Figure 3d). BLI measurements confirmed that many peptides bind to both domains with similar affinities (Table 3). A further 42 Homer motif-matching peptides contain an N-terminally overlapping Ena/VASP motif in a frame that does not structurally align to the Ena/VASP binding mode, that is, a match to $^{-2}$**[FWYL]PΦ**PPx[FWY]^4 or $^{-1}$**[FWYL]**PPPP[FWY]^4 (Figure 3b). While many peptides within these classes were similarly capable of binding Homer1 EVH1, these peptides showed a slight bias toward binding ENAH EVH1, based on their distribution of SPOT intensities (Figure 3c,d).

2.5 | A single motif-flanking residue modulates binding to Homer1

Of the 140 peptides that contain overlapping Ena/VASP and Homer motifs that we tested, 58 bound detectably to Homer1 and 55 to ENAH EVH1. Most peptides were not highly specific, with 46 peptides binding to both domains. Several peptides exhibited modest selectivity in the SPOT array assay, such as FAT1 (FPPPPEDF) and ASPP2 (YPPPPY), which bound to ENAH two- to three-fold better than Homer1 EVH1. FAT1 also demonstrated a near 10-fold preference for ENAH ($K_D = 13.7 \pm 0.3$ μM) over Homer1 ($K_D = 98 \pm 7$ μM) via BLI, corroborating the differences in SPOT intensity (Table 3). The weak affinity of Homer1 EVH1 for FAT1 is surprising given the presence of both a canonical PPxxF motif and an Ena/VASP-like flank, and we hypothesized that features in the motif-surrounding sequence may disfavor the FAT1–Homer1 interaction.

To identify potential negative design elements, we created logos for the sequences that bound specifically to Homer1 or ENAH EVH1 domains by SPOT array. This revealed that Homer1, but not ENAH, disfavored Pro at position 5, immediately C-terminal to the core Homer motif (Figure 4a). Notably, both FAT1 and ASPP2 encode a Pro in this position. The crystal structure of Homer2

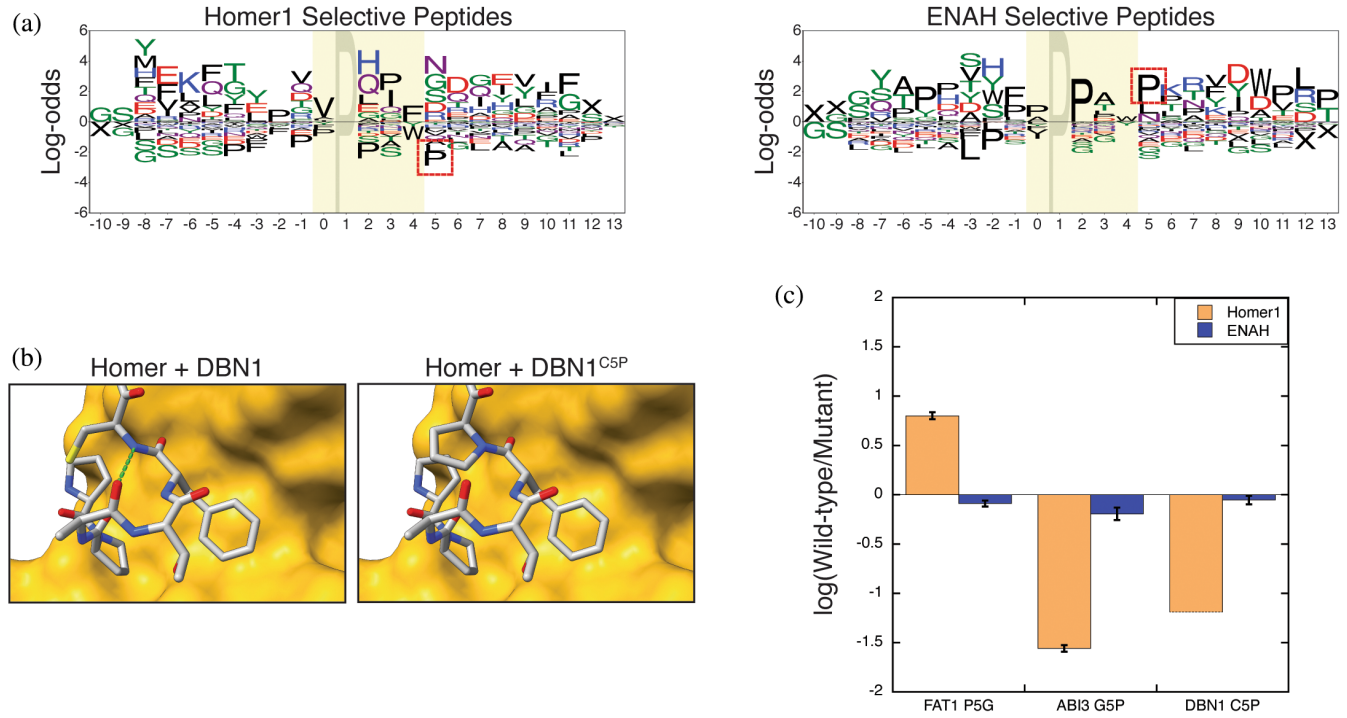

FIGURE 4 (a) Logos for peptides containing the extended Homer motif that preferentially bound to EVH1 domains from Homer1 (left) or ENAH (right) on SPOT arrays. Sequences are aligned by their Homer1 motif. The red box indicates the position of the Pro^5 that serves as a Homer1 negative element. (b) The structure of Homer2 EVH1 domain bound to a peptide from DBN1 demonstrates that the residue in position 5, when not Pro, can hydrogen bond (green) with the residue in position 3 (5ZZ9) (Li et al., 2019). (c) The fold-change in binding affinity of ENAH and Homer1 EVH1 domains for peptides in which a Pro was removed ($FAT1^{P5G}$) or introduced ($ABI3^{G5P}$, $DBN1^{C5P}$) in the position following the Homer1 motif.

bound to a peptide from DBN1 (PDB: 5ZZ9) shows that this residue, when not Pro, can hydrogen bond with the residue in position 3 (Figure 4b) (Li et al., 2019). This interaction may orient the aromatic residue in position 4 for docking within P_H. Removing this element from FAT1 (P5G) yielded a peptide that bound six-fold tighter to Homer1 EVH1, but this mutation had almost no effect on ENAH binding (Figure 4c). Similarly, introducing Pro at this position in peptides from ABI3 (G5P) and DBN1 (C5P) substantially decreased the affinity for Homer1 EVH1, with minimal impact on ENAH binding. Proline at position 5 is an elegant example of a structural strategy that can increase the binding specificity of peptide segments that match both the Ena/VASP and Homer binding motifs.

2.6 | Mutational transformation of EVH1 binding preferences

Co-crystal structures of Ena/VASP and Homer EVH1 domains bound to representative ligands have revealed residues within the binding sites that appear crucial for defining the reported binding motifs. To identify the extent to which a small set of residues is responsible for favoring distinct binding motifs, we attempted to convert the binding preferences of Homer1 and ENAH by swapping four binding site residues in ENAH, representing 5% of the differences between these domains ($ENAH^{Homer1\text{-}like}$; M14F/Y16I/R81A/N90G) (Figure 5a). As demonstrated by a single-substitution SPOT array analysis of the promiscuous peptide from ABI3, ENAH was most sensitive to substitutions within the Ena/VASP motif ($^{-3}$LPPPP^{1}), whereas Homer1 was sensitive to substitutions within the Homer motif (^{0}PPPGF^{4}) (Figure 5b). The tolerance for deviations from the canonical motifs for each domain, and the inability to resolve the expected contribution of N-terminal residues to Homer1 binding, is likely due to testing a high-affinity ligand in a multivalent context. Notably, $ENAH^{Homer1\text{-}like}$ exhibited Homer1-like binding properties, both in terms of the decreased sensitivity to substitutions in the Ena/VASP motif and the acquired requirement for a large hydrophobic residue at position 4 (Figure 5d). Unlike Homer1, $ENAH^{Homer1\text{-}like}$ had a strong preference for valine at position 4, implying that additional differences between these domains are responsible for fine-tuning the motif. Nevertheless, the ability to recapitulate most Homer1 preferences within a markedly different background verifies that just a few residues play a pivotal role in defining EVH1 domain specificity.

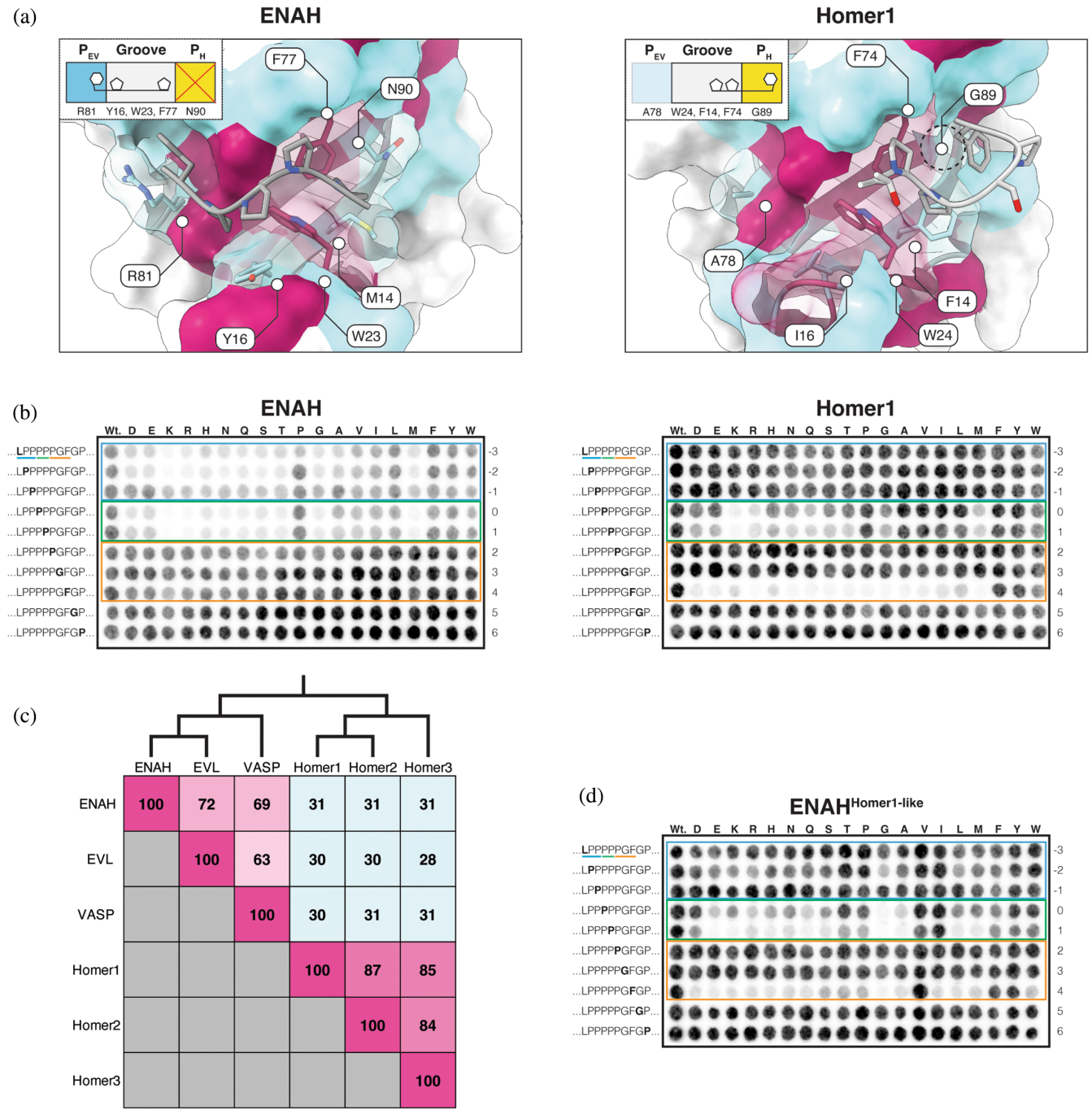

FIGURE 5 (a) ENAH (EVH1) and Homer1 (1DDV) in complex with their representative ligands. Residues within 7 Å of the binding site are colored by whether they are shared (maroon) or different (cyan) between these paralogous domains (Beneken et al., 2000; Prehoda et al., 1999). (b) Mutational analysis of the overlapping motif in ABI3 binding to ENAH and Homer1 EVH1 domains (blue = Ena/VASP-like flank, green = overlapping prolines, yellow = Homer-specific motif residues). In each row, the substituted residue is marked in bold text. (c) Percentage identity matrix of the human Ena/VASP and Homer family EVH1 domains. The tree clusters domains by pairwise sequence identity. (d) Mutational analysis of the overlapping motif in ABI3 binding to the ENAH$^{\text{Homer1-like}}$ EVH1 domain.

2.7 | An ortholog from *Dictyostelium discoideum* sheds light on the evolution of EVH1 binding preferences

Ena/VASP and Homer are highly conserved in metazoans, and both families are present in choanoflagellates, the single-cell organisms most closely related to metazoans (Burkhardt et al., 2014). Several phylogenetically remote amoebas lack Homer proteins but encode a singular Ena/VASP protein, as defined by the presence of both EVH1 and EVH2 domains. We hypothesized that these orthologs, which may resemble the ancestral EVH1

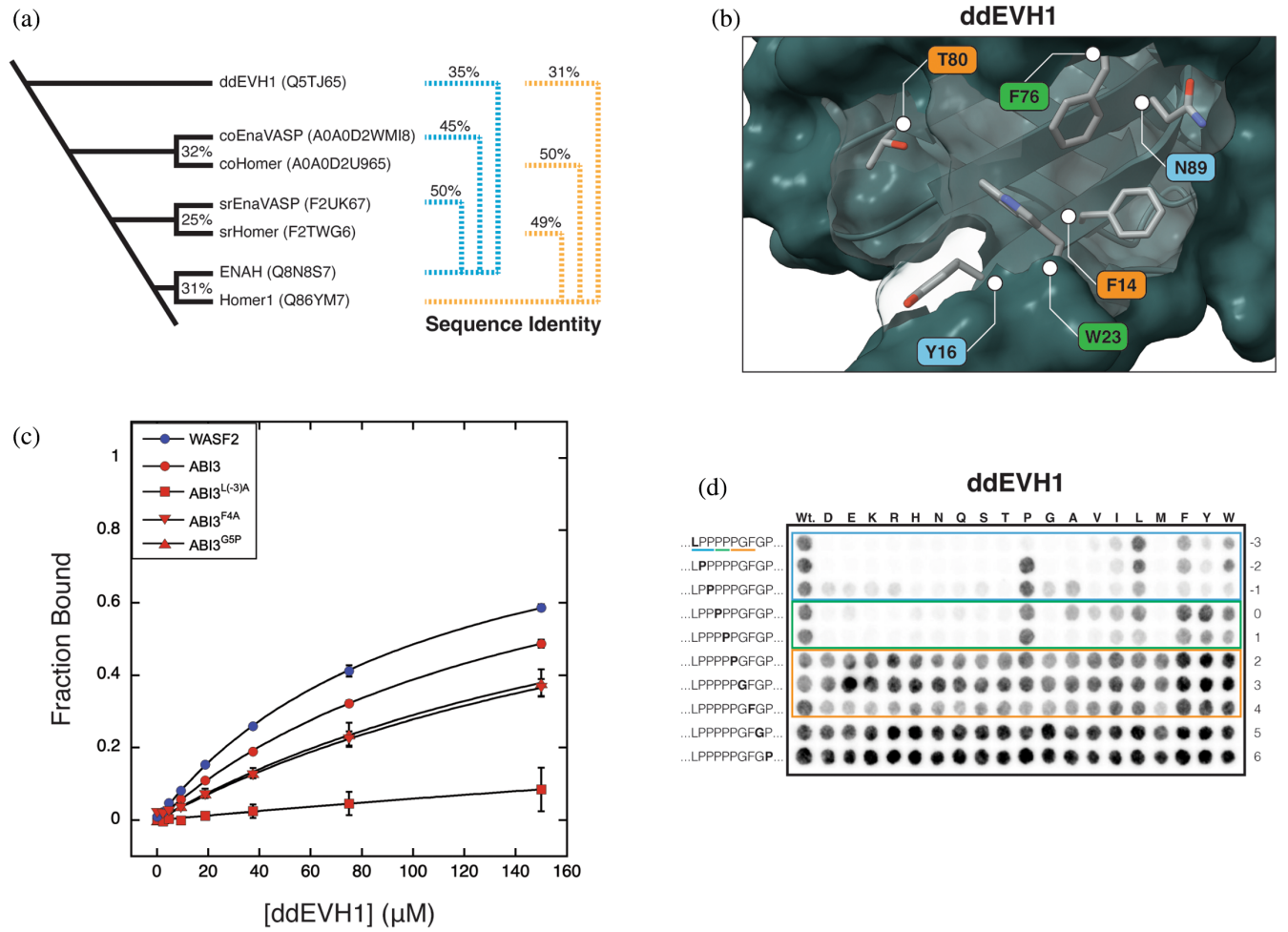

FIGURE 6 (a) Dendrogram representing the positioning of diverse organisms containing Ena/VASP and Homer proteins along the tree of life. The sequence identity for Homer EVH1 domains (and ddEVH1) is shown relative to human Homer1 (yellow), and the sequence identity for Ena/VASP EVH1 domains is shown relative to human ENAH (blue). (b) AlphaFold2 structural model of ddEVH1 (Q5TJ65). The color of each label reflects whether the residue is similar to the corresponding residue in Homer (yellow), Ena/VASP (blue), or both (green). (c) BLI measurements for ddEVH1 binding to peptides from WASF2 and ABI3. (d) Mutational analysis of the overlapping motif in ABI3. SPOT array labels and boxed areas are as in Figure 5. BLI, biolayer interferometry.

domain prior to the gene duplication event that gave rise to Homer, may offer insight into the evolution of binding specificity within this paralogous family.

The soil-dwelling amoeba *D. discoideum*, the Ena/VASP protein, ddVASP, is required for filopodia formation, chemotaxis, and macroendocytosis (Han et al., 2002; Körber and Faix, 2022). As assessed by sequence identity, the *D. discoideum* EVH1 domain (which we refer to here as ddEVH1) is similarly diverged from the human Ena/VASP and Homer EVH1 domains, with 35% and 31% sequence identity, respectively (Figure 6a). An AlphaFold2 model of ddEVH1 reveals that the region corresponding to the peptide binding site in Ena/VASP and Homer exhibits a blend of features from both human protein families (Figure 6b) (Jumper et al., 2021; Mirdita et al., 2022). Like Homer, but not Ena/VASP, ddEVH1 lacks a well-formed P_{EV} ($T80_{ddEVH1}$ and $A78_{Homer1}$ vs. $R81_{ENAH}$). Like Ena/VASP, but not Homer, ddEVH1 has an occluded P_H ($N89_{ddEVH1}$ and $N90_{ENAH}$ vs. $G89_{Homer1}$). Additionally, whereas Ena/VASP and Homer1 EVH1 domains each contain three aromatic residues in the proline binding groove, ddEVH1 contains a tetrad that includes both the unique Ena/VASP ($Y16_{ddEVH1}$ and $Y16_{ENAH}$ vs. $I16_{Homer1}$) and Homer ($F14_{ddEVH1}$ and $F14_{Homer1}$ vs. $M14_{ENAH}$) aromatic residues. Sequence analysis of the Ena/VASP proteins from other amoebas demonstrates that this binding site architecture is highly conserved (Figure S5 in Data S1).

We tested ddEVH1 for binding to several human peptides identified in this study (Figure 6c). Like ENAH and Homer1 EHV1 domains, ddEVH1 bound to peptides from ABI3 and WASF2, though the affinity for each was weak ($K_D > 100$ μM). Alanine substitution of the N-terminal Leu^{-3} ($^{-3}$**L**PPPPPGF^{-4}) in ABI3 ($ABI3^{L(-3)A}$)

abrogated ddEVH1 binding, while substitution of the C-terminal Phe[4] (ABI3^{F4A}), or replacement of the motif-trailing Gly[5] with Pro (ABI3^{G5P}), had modest effects on binding. In these ways, the ddEVH1 binding preferences are similar to those of the human Ena/VASP EVH1 domain, despite, like Homer1, containing differences in key binding site residues. Nevertheless, ddEVH1 bound poorly to the ENAH-binding peptides from DBN1 and FAT1 (data not shown).

Single-substitution SPOT analysis of ABI3 demonstrated that, in contrast to ENAH, ddEVH1 strongly preferred Leu over an aromatic residue at position −3 (Figure 6d). This is likely caused by the absence of cation-pi interactions formed in ENAH by R81$_{ENAH}$ and may explain the weak binding of ddEVH1 to FAT1 ($^{-3}$**F**PPPPEDF[4]). The array also revealed that ddEVH1 has a stronger preference than ENAH for proline residues at positions −2 through 1. This may indicate that the proline binding groove, with its extra aromatic residue, compensates for a poorly formed P_{EV} pocket. DBN1, which does not bind to ddEVH1, lacks a proline at the −1 position ($^{-3}$LP**E**PPATF[4]). Lastly, ddEVH1 exhibits a weak sensitivity to the replacement of Phe[4] with a nonaromatic residue, which aligns with our finding that alanine substitution at this position (ABI3^{F4A}) weakened binding, as measured by BLI. This preference is surprising, given the absence of P_H that accommodates the binding of this residue to Homer EVH1 domains.

Our biochemical characterization of ddEVH1 suggests a preference for the motif [LF]PPPP, with less tolerance for deviation within this sequence than is observed for human Ena/VASP orthologs. In *D. discoideum*, 113 proteins contain an [FL]PPPP motif. Of these, 22 have human orthologs, with several annotated as participating in actin regulation or neuronal processes (Table S3). Furthermore, the ABI protein in *D. discoideum*, a known binding partner of ddEVH1, contains six copies of the sequence [LF]PPPP (UniProt ID: Q55FT9) (Litschko et al., 2017). This fact, together with our observation that peptides matching this motif bind ddEVH1 an order of magnitude weaker than ENAH and Homer1 EVH1, suggests that multivalency may be crucial for obtaining physiologically relevant binding affinities in amoeba Ena/VASP systems.

2.8 | A Homer ortholog from *Capsaspora owczarzaki* can discriminate against ENAH motifs

The incomplete divergence of the Ena/VASP and Homer binding profiles may imply that evolutionary paths to distinct interactions are long (requiring many mutations) or rare (requiring specific combinations of mutations), such that fully differentiated binding properties are unlikely to arise. This could be the case, for example, if most mutations that lead to diverged binding compromise the structural integrity of the domain. The advent of multicellularity provided a new mechanism by which biological systems can spatiotemporally restrict the co-localization of proteins, segregating proteins into distinct niches without the need for divergence at the level of molecular recognition. Given the potential for deleterious competition between Ena/VASP and Homer, we hypothesized that unicellular organisms may face greater pressure to diverge their interface residues.

Our search for orthologs in single-cell species identified both an Ena/VASP and Homer protein in the eukaryote *C. owczarzaki*, a member of the Filasteria clade, the sister group to choanoflagellates and metazoans (Figure 6a). The EVH1 domain in the Homer protein, which we call coHomer, shares 50% sequence identity to human Homer1. While AlphaFold2 modeling suggests that the architecture of the proline groove and P_H are nearly identical to Homer1, coHomer uniquely incorporates an acidic residue (E78) within the P_{EV} pocket (Figure 7a). This mutation may disfavor the engagement of peptides that bind well to Ena/VASP by disrupting the docking of a hydrophobic residue in P_{EV} or by repelling peptides containing acidic residues often found upstream of the motif in Ena/VASP binders (Niebuhr et al., 1997).

We compared the binding of multiple peptides to Homer1 and coHomer EVH1 domains using BLI (Figure 7b). Peptides that bind to ENAH EVH1 and include acidic residues within a 5-residue window N-terminal to the motif (ABI3, DBN1, and FAT1^{P5G}) bound to coHomer with at least a 10-fold reduction in affinity compared to Homer1 (Table 4). DVL3, which contains an overlapping motif but lacks N-terminal acidic residues, also exhibited reduced binding affinity. A peptide from RAX that lacks the Ena/VASP P_{EV} docking residue at position -3 ($^{-3}$**[FWYL]**PxΦP[1]), bound equivalently to both Homer1 and coHomer. This trend suggests that coHomer disfavors binding to Ena/VASP-binding peptides largely by repelling N-terminal acidic residues, but also because of a charge in P_{EV}. Introducing a corresponding glutamate into the Homer1 EVH1 domain (Homer1^{A78E}) was insufficient to evoke the observed binding differences between Homer1 and coHomer (Figure S6A in Data S1). However, this may be due to less-dense packing and thus greater flexibility of Glu in Homer1 compared to the corresponding residue in coHomer (Figure S6B in Data S1). While multiple mutations may be required to define distinct coHomer versus Homer1 binding preferences, our results demonstrate

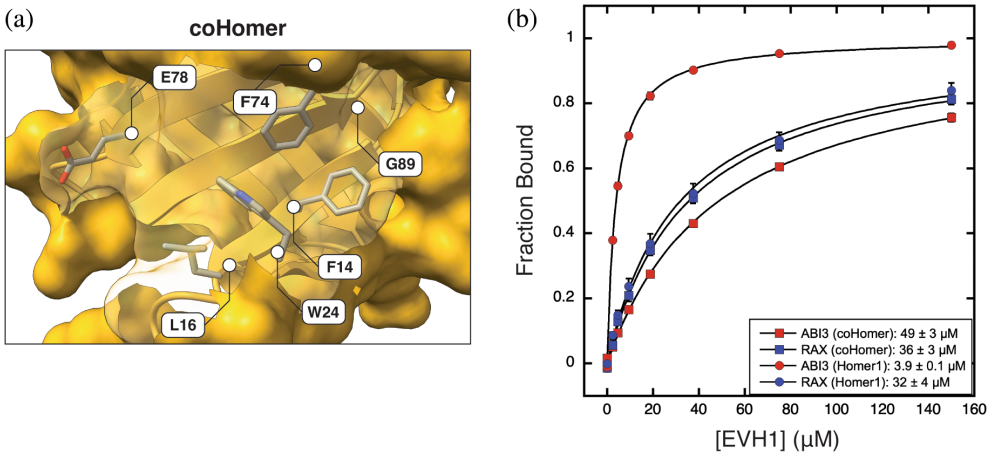

FIGURE 7 (a) AlphaFold2 structural model of coHomer (UniProt: A0A0D2U965). (b) BLI binding curves comparing EVH1 domains from Homer1 (circle) and coHomer (square) binding to peptides from ABI3 and RAX (sequences in Tables 1 and 2). BLI, biolayer interferometry.

TABLE 4 Binding affinities of peptides for coHomer, measured by BLI.

Protein name	Peptide sequence	K_D (μM)
DBN1	LNFDE**LPEPPATF**CDPEEVE	>150
FAT1^{P5G}	DIESD**FPPPPEDF**GAADELP	>150
ABI3	GDELG**LPPPPPGF**GPDEPSW	49 ± 3
RAX	GFGPPAQSLPASYTPPP**PPPPF**LNSPPLGPGLQPLA	36 ± 3
DVL3	PLPHPGAAPWPMAFPYQ**YPPPPHPY**NPHPGFPELGY	>150

Note: Values represent the average and standard deviation of three replicates. The Homer motif, or extended motif if present, are highlighted in bold.
Abbreviation: BLI, biolayer interferometry.

that further diverged molecular recognition profiles for Homer and Ena/VASP are evolutionary accessible but have not been selected for in metazoan lineages.

3 | DISCUSSION

3.1 | Homer1 binding preferences

Homer, a constitutive tetramer, carries out its biological function by crosslinking (or, in the case of immediate early monomeric Homer isoforms, disassembling) complexes of partners using its EVH1 domain (Shiraishi-Yamaguchi and Furuichi, 2007). Identifying these binding partners is key to understanding the biological role of Homer proteins. Because of the relatively weak affinity of EVH1-mediated binding and the dynamic nature of the postsynaptic density, many of these interactions are likely transient and only populated in response to specific stimuli. For this reason, Homer-mediated interactions may evade standard techniques for identifying native protein–protein interactions, and this may explain the low recovery of annotated binding partners in various Homer co-IP mass spectrometry studies (Goulding et al., 2017; Stillman et al., 2022). These studies are also limited by a focus on a single tissue type, despite the wider expression of Homer (Xiao et al., 1998).

Most Homer binding partners have been identified in low-throughput, candidate-driven studies by virtue of the inclusion of a PPxxF motif, first identified in metabotropic glutamate receptors (Brakeman et al., 1997; Tu et al., 1998). This led to the circular reinforcement of PPxxF as the Homer binding motif, potentially excluding partners that lack this sequence. Several deviations from this motif have been noted in the literature, but this has not led to a broader exploration of Homer binding preferences (Rong et al., 2003; Yuan et al., 2003).

In this study, we screened T7-pep to identify Homer1 EVH1 binders and uncovered features that support binding. Our results demonstrate that the reported core Homer motif, PPxxF, is overly restrictive, and sequences matching a more general motif [PIALV]Pxx[FWY] can bind to the Homer1 EVH1 domain. While deviations from PPxxF may result in lower-affinity motifs (as in peptides from CAP2, WIPF2), these sequences may be relevant in avid contexts, such as multimeric complexes or proteins containing several motifs (Bugge et al., 2020). Notably, full-length CAP2 and WIPF2 contain multiple instances of both canonical and noncanonical Homer motifs.

Additionally, we identified specific examples of how the sequence context flanking the core motif, such as a leading Ena/VASP-like segment or a trailing proline, can modulate the affinity and specificity of this interaction. These findings build on and contextualize the previous discoveries that many Homer ligands contain an N-terminal, affinity-enhancing Leu, and that mutation of an N-terminal FPP diminishes the binding of Homer3 to FAT1 (Li et al., 2019; Schreiner et al., 2006). By combining our findings and reported Homer preferences from the literature, we defined an updated Homer motif [fwyl]pp[PIALV]P..[FWY][^p][dn], where uppercase letters reflect obligate positions and lowercase letters indicate positive and negative (indicated by "^") elements that can alter affinity (Barzik et al., 2001; Li et al., 2019).

3.2 | The evolution of binding preferences in EVH1 domains

Homer and Ena/VASP EVH1 domains share a common ancestor, and both families are present in the premetazoan *S. rosetta*, indicating that the family-expanding duplication event predated the emergence of metazoans some 600 million years ago (Figure 6a, Figure S4 in Data S1) (Ayala et al., 1998). Many amoebas, further remote from metazoans, encode a singular Ena/VASP protein but lack Homer orthologs. Thus, we hypothesized that EVH1 domains from amoebas may be good representatives of the ancestral domain.

The EVH1 domains from amoebas share near-equal sequence identity with domains from human Ena/VASP and Homer. Furthermore, the binding site architecture of these domains blends features from both human families. While we cannot rule out that the binding preferences of these EVH1 domains may have drifted over time, proteins at the center of interaction networks are buffered against drift due to the extensive coevolution required to maintain their interactomes (Fraser et al., 2002, 2003; Hahn and Kern, 2005; Makino and Gojobori, 2007). In support of this, even those EVH1 domains from amoebas with low sequence identity share the binding site residues we identified as key for defining motif preferences, suggesting the persistence of a common binding mode (Figure S5 in Data S1). Together, these observations suggest a model whereby the subfunctionalization of an ancestral binding site similar to that in ddEVH1 birthed distinct Ena/VASP and Homer families.

In support of this model, we observed that ddEVH1 binds weakly to the motif [FL]PPPP and exhibits a slight preference for the C-terminal aromatic residue found in the Homer motif. Seemingly, selective reinforcement of preexisting preferences for hydrophobic residues flanking the prolines, as opposed to de novo emergence, established the higher-affinity motifs recognized by metazoan EVH1 domains (Figure 8). As evidenced by the affinity of Homer1 for sequences containing an Ena/VASP-like N-terminal flank, Homer did not lose its preference for the ancestral motif, which exists independent of a well-formed P_{EV}. Similarly, despite lacking a distinct P_H, the ENAH EVH1 domain can utilize this site to bind to a motif-trailing proline in ABI1 ($^{-3}$FPPPPPP**P**P^{4}) (Hwang et al., 2022).

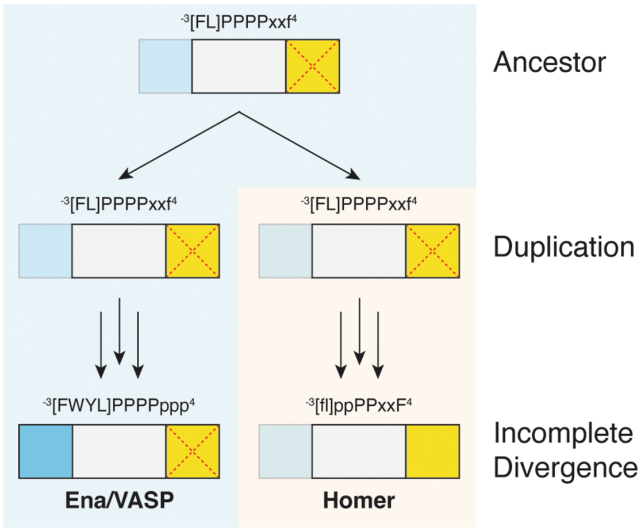

FIGURE 8 An evolutionary model of EVH1 divergence. Uppercase letters reflect obligate positions and lowercase letters indicate positive elements that enhance the affinity of this interaction. The EVH1 ancestor of Ena/VASP and Homer likely bound to a motif like that preferred by ddEVH1, with a poorly formed P_{EV} (transparent) and occluded P_H (red cross mark). Incomplete subfunctionalization of the core binding site resulted in a Homer EVH1 domain that retained its preference for an Ena/VASP-like N-terminal flank.

Interestingly, negative design elements did not arise to eliminate binding overlap between the human Ena/VASP and Homer families. These EVH1 domains may not have diverged further because changes that enhance selectivity compromise binding. However, the sole Homer protein in the premetazoan *C. owczarzaki* robustly discriminates against sequences containing an Ena/VASP motif and N-terminal acidic residues, demonstrating that further diverged binding profiles are accessible. Why then did the Homer preference for the Ena/VASP-like flank persist in metazoan lineages? We posit that the retention of this preference in Homer is either (a) functionally beneficial or (b) neutral with respect to fitness but preserved due to constraints on drift, such as those arising from high interaction connectivity.

3.3 | Rationalizing overlap in the Ena/VASP and Homer recognition landscape

SLiMs play pivotal roles in cellular physiology, and mutations that disrupt these sequences can reduce fitness and lead to disease (Uyar et al., 2014; Van Roey et al., 2014). Fitness can also be compromised by competition between proteins for binding, leading paralogs to develop specificity niches, either by diverging their molecular recognition profiles or by spatiotemporal compartmentalization (Ghose et al., 2023; McClune and Laub, 2020; McClune et al., 2019). Yeast SH3 domains provide examples of both strategies (Cesareni et al., 2002; Landgraf et al., 2004). A peptide from the protein Pbs2 binds to the Sho1 SH3 domain with high specificity, indicating that specificity can be encoded in molecular recognition (Zarrinpar et al., 2003). On the other hand, a peptide from Pex14 binds promiscuously to a number of SH3 domains, but it is sequestered with its cognate SH3 domain (Pex13) in the peroxisome. Similarly, the Ena/VASP and Homer EVH1 domains have diverged their recognition profiles sufficiently that they can engage specific, non-promiscuous ligands. Peptides that bind to both Ena/VASP and Homer may be spatiotemporally restricted from encountering both simultaneously.

It is also possible that overlapping binding preferences confer a benefit. The intricate landscape of cellular processes depends on conditional interactions, which can be achieved by direct competition for binding sites (Van Roey et al., 2012, 2013). For example, Homer3 and calcineurin compete for binding to NFATc2, and competitive binding between constitutively expressed tetrameric Homer and the immediate early monomeric isoform is central to Homer function (Clifton et al., 2019; Huang et al., 2008; Xiao et al., 1998). Competitive interactions with Ena/VASP proteins may play a similar role for motifs that bind to both families.

Several proteins that contain peptides that bind both domains stand out as candidate functional partners for both Ena/VASP and Homer based on localization, interaction, and GO term data (Figure S3 in Data S1). Among these are ABI3 and WASF2, two members of the pentameric WAVE complex that regulates Arp2/3 mediated actin polymerization (Rottner et al., 2021). The WAVE complex interacts directly with Ena/VASP proteins to drive enhanced actin assembly, and this association is conserved as far back as *D. discoideum* (Chen et al., 2014; Litschko et al., 2017). Given the role of Homer in synaptic plasticity, which is an actin remodeling event, a direct connection between Homer and the actin polymerization machinery is conceivable. Circumstantial evidence suggests that Homer proteins may also interact with the WAVE complex. In neurons, the WAVE complex plays a crucial role in orchestrating the development of diverse actin-filament protrusions (Soderling et al., 2007). ABI3 has been shown to regulate dendritic spine morphology and synapse formation, and a peptide from ABI3 is the tightest Homer1 binder identified in this study ($K_D = 3.9 \pm 0.1$ μM) (Bae et al., 2012). Through its interaction with various proteins, Homer can influence both the emergence and maturation of dendritic spines (Sala et al., 2001; Yoon et al., 2021). Homer3 knockdown in neutrophils impairs the recruitment of the WAVE2 complex to the leading edge of motile cells (Wu et al., 2015). In the cerebral cortex of mice, Homer1 dissociates from a complex containing the Arp2/3 members ARPC2, 4, and 5 in an activity-dependent manner (Stillman et al., 2022).

The small number of interface residues that constitute SLiM-mediated interactions makes them highly amenable to regulation by post-translational modification. Motif phosphorylation is a well-documented switch for SLiM binding (e.g., phosphorylation of the NPxY motif in the integrin $\beta 3$ subunit shifts binding from Talin to Dok1) (Oxley et al., 2008; Van Roey et al., 2012). Phosphorylation can also modulate the affinity of a motif, and phosphorylation of the non-interface Ser and Thr residues in the mGlur5 Homer binding peptide (TPPSPF) by Cdk5 increases affinity for Homer1 (Orlando et al., 2009). Our study uncovered that Homer1 can bind to sequences containing Tyr^4 within the core motif but is intolerant of acidic residues at this position, implying that phosphorylated Tyr^4 would not support binding. However, in the context of an overlapping motif, this modification may enhance binding to Ena/VASP, given the preference for motif-flanking negative charges (Niebuhr et al., 1997). Of the 46 dual-binding peptides identified in this study, 20 contain Tyr^4, and 5 of these residues are annotated as phosphorylation sites (Hornbeck et al., 2012). One of these proteins, the non-receptor kinase activated CDC42 kinase 1 (TNK2) has a documented role in neurite migration, and phosphorylation of this Tyr plays a role in glioma oncogenesis (La Torre et al., 2013; Zhang et al., 2015).

Proline is unique in its ability to populate *cis*-peptide bonds (Reimer et al., 2014). The relative populations of *cis* versus *trans* states, which can be modulated by surrounding residues, may impact ENAH versus Homer1 EVH1 binding. Greenwood et al. (2014) studied the conformation of the Trp^{-3}-Pro^{-2} amide bond in the VASP-binding motif $^{-3}$WPPPP^1 and found approximately equal populations of the *cis* and *trans* conformations in the unbound peptide, but EVH1 binding only to the *trans* isomer. Notably, when bound to Homer1 EVH1, the Ser^2-Pro^3 bond in a peptide from mGlur5 (^{0}PP**SP**F^4) adopts a *cis* conformation to position Phe^4 in the P_H pocket (Beneken et al., 2000). In contrast, Pro^2-Pro^3 in peptide

$^{-3}$FPPPP**PP**PP^{5} from Abi1 adopts a *trans* conformation when bound to ENAH EVH1 that allows domain contacts with prolines in positions −2, 1, and 4, in a polyproline-II helix conformation (Hwang et al., 2022). In disordered peptides, an aromatic residue either preceding or following a proline favors the *cis* state, whereas tracts of prolines favor *trans* conformations (Zondlo, 2013; Urbanek et al., 2020). Thus, Homer1 motifs that include ^{2}XPF^{4} (X = non-proline) may preferentially populate a Homer1-favoring *cis* state, whereas motifs including multiple prolines in positions 1–3 may populate an ENAH-favoring *trans* state. Although NMR analysis of the conformations adopted by different ligands studied here would be required to test this idea rigorously, trends from our screening and array data support that conformational biases may impact selectivity. For example, Figure 2d shows that when analyzing all Homer1 binders from the screen, Pro is enriched at both positions 2 and 3. However, Figure 4a shows that in Homer1-selective binders, Pro is enriched in position 3 but not position 2. Position 3 is likely to be in a *cis* state when preceded by a non-proline residue and followed by an aromatic residue, setting up a conformation like that in the mGluR5 complex. In contrast, ^{1}PPP^{3} is likely to be configured as an all-trans PP-II helix favorable for ENAH binding. In the cell, catalyzed *cis-trans* isomerization could provide a mechanism to modulate binding kinetics.

In summary, our results suggest that the Homer interaction landscape remains only partially explored, and we present new motif definitions and candidate binding partners to facilitate the discovery of novel interactions. Furthermore, our data provide insight into the evolution of molecular specificity in SLiM binding domains, documenting incomplete divergence within this paralogous family of domains. Residual binding overlap may be a strategy to regulate molecular decision-making at the post-synaptic density. The residual similarities and subtle differences between Homer1 and Ena/VASP EVH1 domains also have ramifications for the design of family-specific EVH1 inhibitors.

4 | METHODS

4.1 | Protein constructs and purification (BLI constructs)

EVH1 domains used for BLI experiments were cloned into a pMCSG7 vector for recombinant expression in *E. coli* (Table S4). The plasmid was transformed into Rosetta2(DE3) cells (Novagen) and grown in 1 L Terrific Broth (TB) media with 100 μg/mL ampicillin. Cells were grown while shaking at 37°C until an OD600 of 0.5–0.6, upon which the cultures were placed on ice for 20 min. Following this, protein expression was induced with 0.5 mM isopropyl β-D-1-thiogalactopyranoside (IPTG) and the induced cells were grown by shaking at 18°C overnight. Cultures were harvested by centrifugation, and the resulting pellets were resuspended in lysis buffer (20 mM HEPES pH 7.6, 500 mM NaCl, 20 mM imidazole) at a concentration of 0.2 g/mL before being frozen at −80°C.

The next day, the pellets were thawed and supplemented with 0.2 mM phenylmethylsulfonyl fluoride (PMSF) protease inhibitor. The cells were lysed by sonication, centrifuged, and the resulting supernatant was incubated with 2 mL Ni-NTA resin (washed in lysis buffer) while rotating at 4°C. After 1 h, the resin was washed twice with 20 mL lysis buffer. The protein was eluted from the Ni-NTA resin with 8 mL elution buffer (20 mM HEPES pH 7.6, 500 mM NaCl, 300 mM imidazole). TEV protease was added to the sample at an approximate concentration of 1 mg TEV:50 mg EVH1. The sample was dialyzed overnight at 4°C in 1 L of TEV buffer (50 mM HEPES pH 7.5, 300 mM NaCl, 0.5 mM EDTA, 2 mM DTT).

The completeness of the TEV reaction was assessed by sodium dodecyl-sulfate polyacrylamide gel electrophoresis (SDS-PAGE). Next, the sample was applied to 2 mL Ni-NTA resin and washed with 8 mL lysis buffer. The flow-through and wash were pooled, filtered, and loaded onto an S75 26/60 sizing column equilibrated in gel filtration buffer (20 mM HEPES pH 7.6, 150 mM NaCl, 1 mM DTT). Fractions were collected and their purity was assessed via SDS-PAGE. Pure samples were pooled and concentrated prior to being flash-frozen and stored at −80°C.

4.2 | Protein constructs and purification (surface display constructs)

EVH1 domains used for bacterial cell surface display and SPOT arrays were cloned into a pDW363 vector for recombinant expression in *E. coli* (Table S4). The plasmid was transformed into Rosetta2(DE3) cells (Novagen) and grown in 1 L TB media with 100 μg/mL ampicillin and 0.05 mM D-(+)-biotin for in vivo biotinylation. Protein expression was carried out as above.

Pellets were thawed and supplemented with 0.2 mM PMSF prior to lysis by sonication. The lysed sample was centrifuged, and the resulting supernatant was incubated with 2 mL Ni-NTA resin (washed in lysis buffer) while rotating at 4°C. After 1 h, the resin was washed twice with 20 mL lysis buffer. The protein was eluted from the Ni-NTA resin with 8 mL of elution buffer (20 mM

HEPES pH 7.6, 500 mM NaCl, 300 mM imidazole). The eluted sample was filtered and loaded onto a S75 26/60 sizing column equilibrated in gel filtration buffer (20 mM HEPES pH 7.6, 150 mM NaCl, 1 mM DTT, 5% glycerol). Fractions were collected and their purity assessed via SDS-PAGE. Pure samples were pooled and concentrated prior to being flash-frozen and stored at −80°C.

4.3 | Protein constructs and purification (SUMO peptides)

Peptides were cloned as SUMO fusion constructs and inserted into a pDW363 vector for recombinant expression in *E. coli*. The construct was transformed into Rosetta2 (DE3) cells (Novagen) and grown in Lysogeny broth (LB) media supplemented with 100 μg/mL ampicillin and 0.05 mM D-(+)-biotin for in vivo biotinylation. The cells were grown while shaking at 37°C until reaching an OD600 of 0.7, upon which protein expression was induced with 1 mM IPTG at 37°C for 5 h. Cultures were harvested by centrifugation, and the resulting pellets were frozen overnight at −80°C. The next day, the pellets were thawed and resuspended in 4 mL B-PER (Thermo Fisher)/g cell pellet and supplemented with 0.2 mM PMSF. Samples were incubated at room temperature for 15 min, spun down, and the supernatant was loaded into columns containing 0.4 mL Ni-NTA resin equilibrated in wash buffer (20 mM Tris pH 8.0, 500 mM NaCl, 20 mM imidazole). The columns were washed 3× with 1 mL wash buffer and then eluted from the column with 1.5 mL elution buffer (20 mM Tris, 50 0 mM NaCl, 300 mM imidazole pH 8.0). Samples were flash-frozen and stored at −80°C.

4.4 | Surface display constructs

Control peptides for bacterial surface display were cloned as C-terminal fusions to the surface protein eCPX using a vector designed by the Daugherty group (Rice and Daugherty, 2008). Peptides were flanked by a C-terminal c-Myc tag and by an N-terminal FLAG tag that was used for quantification of peptide expression on the bacterial surface (Table S4). These plasmids were transformed into chemically competent MC1061 *E. coli* cells for FACS analysis.

The T7-pep library, consisting of the same construct design detailed above, was transformed into electrocompetent MC1061 cells (Lucigen) to maximize transformation efficiency (Larman et al., 2011); 25 μL of cells were pre-chilled on ice for 10 min. These cells were mixed with plasmid and were pulsed in a 0.1 cm cuvette at 1.8 kV, 600 Ω, 10 μF using a Biorad electroporator. The cuvette was immediately rinsed twice with 1 mL of Super Optimal Broth media with 20 mM glucose (SOC) that had been pre-warmed at 37°C. A serial dilution of the transformed cells was plated on LB + chloramphenicol (Cm) plated to assess transformation efficiency. The cells were recovered at 37°C for 1 h and then combined with 40 mL LB + Cm + 0.2% glucose for overnight growth. Cells were retransformed between rounds of enrichment to minimize the possibility of clones developing growth advantages associated with mutations in the chromosomal DNA.

4.5 | FACS sample preparation

The following protocol was adopted from Hwang et al. (2022). All PBS buffers were supplemented with additional NaCl to a final concentration of 300 mM. Cultures consisting of 5 mL LB + 25 μg/mL Cm + 0.2% glucose (w/v) were inoculated overnight (37°C) with MC1061 cells encoding arabinose-inducible eCPX-peptide fusion constructs. The next morning, cells were pelleted and used to inoculate a fresh culture of LB + 25 μg/mL Cm (no glucose). These cultures were grown to an OD600 of 0.5–0.6 (37°C). Upon reaching this density, eCPX expression was induced with 0.04% arabinose (w/v) for 1.5 h. Following expression, the OD600 was measured again, and an appropriate volume of culture was centrifuged to obtain a pellet of 1×10^7 cells/FACs analysis sample. In the case of T7-pep library sorting, 1×10^8 cells were pelleted. The pellets were washed with PBS pH 7.4 + 0.1% BSA and then incubated with anti-FLAG antibody conjugated to allophycocyanin (anti-FLAG:APC; PerkinElmer) (diluted 1:100 into PBS pH 7.4 + 0.1% BSA; 30 μL/1×10^7 cells) for 30 min at 4°C. Simultaneously, biotinylated monomeric EVH1 domain (1 μM) was pre-tetramerized by incubation with streptavidin-phycoerythrin (SA-PE; Thermo Fisher) for 30 min. The cells were pelleted and washed with PBS pH 7.4 + 0.1% BSA to remove excess anti-FLAG:APC. Cells were pelleted, resuspended in PBS pH 7.4 + 1% BSA at 25 μL buffer/1×10^7 cells, and incubated with pre-tetramerized EVH1 domain at a 1:1 for a final volume of 50 μL/sample for 1 h at 4°C. Following this incubation, the cells were transferred to a pre-wet Millipore MultiScreen 0.22 μm hydrophilic low protein-binding plate and the buffer was removed by vacuum. The cells were then washed twice with 200 μL PBS + 0.1% BSA before being resuspended in 250 μL PBS + 0.1% BSA for FACS analysis or sorting.

4.6 | Flow cytometry and FACS analysis

Single-clone bacterial surface display analysis was carried out on a FACSCanto instrument (BD Biosciences) with

samples prepared as described above. For each sample, 10,000 events were observed. FACS data were processed using the commercially available software FlowJo (FlowJo™ Software for Mac, Version 10.8.1. Ashland, OR: Becton, Dickinson and Company; 2023). Cells were gated on (1) forward scatter height (FSC-H) versus side scatter height (SSC-H) and (2) side scatter width (SSC-W) versus side scatter height (SSC-H). Cells that made it through these two gates were analyzed for their APC and PE signals to quantify peptide expression and EVH1 binding, respectively.

Enrichment sorting of the T7-pep library was carried out on a FACSAria instrument (BD Biosciences). Collected cells were gated three times: (1) FSC-H versus SSC-H, (2) SSC-W versus SSC-H, and (3) APC versus PE. A no-peptide negative control and two positive control peptides of different affinities for Homer1 (from CAP2, DBN1) were used to set the final collection gate. With each round of sorting, the PE voltage was adjusted to ensure a similar percentage of control cells fell within the gate. Samples, prepared as described above, were oversampled at least 10-fold relative to the library population. After the initial round of selection against the naïve T7-pep library, we performed a negative, PE-only sort and collected the nonbinding population in order to eliminate sequences that were binding to PE. Subsequently, we performed three more rounds of positive selection using Homer1 EVH1, for a total of four positive selections. The final round of sorting was performed twice (Sort5a/5b), but for the purpose of analysis, these populations were combined. Sorted cells were collected in SOC media and recovered at 37°C for 1 h. The culture was then combined with LB + 25 μg/mL chloramphenicol + 0.2% glucose (w/v) culture for overnight growth (37°C) and then miniprepped (Qiagen).

4.7 | Illumina amplicon preparation

The plasmids from each round of enrichment sorting were prepared for single-lane Illumina deep sequencing as follows. Miniprepped plasmids from each round of enrichment (100 ng DNA/sample) were PCR amplified with a common forward primer to introduce an i5 Illumina anchor (FWD PCR) and a unique reverse primer to introduce the i7 Illumina anchor and a unique 6-nucleotide index for demultiplexing (REV INDEX X). A complete list of these primers and their sequences is provided in Table S1. Twelve cycles of amplification were carried out with Q5 High Fidelity DNA Polymerase (NEB) using an annealing temperature of 68°C and a 1 min extension at 65°C. The success of this amplification was verified using a 1.5% agarose gel. Each PCR product was purified using a double-sided SPRI bead cleanup (AMPure XP-Beckman). First, a right-sided selection (0.56×) was used to remove large library fragments. The SPRI beads were resuspended in a solution of 2.5 M NaCl and PEG 8000 (20%, w/v), mixed with the PCR products, and then incubated for 5 min at room temperature. Next, the beads were magnetically separated and the supernatant removed. This supernatant was then used to perform a left-sided selection (0.85×) to remove library fragments and adapter dimers. A fresh sample of SPRI beads was resuspended in PEG solution and then combined with the supernatant from the right-handed selection. The beads were then magnetically separated, the supernatant discarded, and washed twice with 200 μL of prechilled 80% ethanol. Following this wash, the ethanol was removed and the beads were dried for 10 min at room temperature. The final sample was eluted from the beads by resuspension in 11 μL of 10 mM Tris pH 8.0 and their concentration measured via NanoDrop. The samples were pooled and submitted for sequencing using a NextSeq500 instrument with paired-end reads.

4.8 | Illumina data processing

Unless noted, an in-house script was used for the following data processing. Forward and reverse reads from Illumina sequencing were merged using the software BBMerge with the default overlap requirement of 12 base pairs and a quality score of 20 (Bushnell et al., 2017). Read counts for each pool were collapsed by amino-acid sequence, and we applied an initial quality filter requiring a sequence length of 36 amino acids as well as an input library read count filter >5. The remaining 741,742 sequences were clustered to remove redundancy using CD-Hit, yielding a final count of 311,560 unique sequences (Li and Godzik, 2006). For each sequence, the raw read count was converted to a frequency (F^{seq}) by dividing by the total number of reads within the respective pool. Sequences that failed to enrich in the first selection against the naive input library were categorized as "non-enriching." For sequences that persisted through the first two rounds of selection, an enrichment score was calculated by taking the area under the curve (AUC) of $f(i)$, the log-transformed frequency between sequential selection rounds (Figure S1A in Data S1):

$$f(i) = \log_2\left(\frac{F_{i+1}^{\text{seq}}}{F_i^{\text{seq}}}\right).$$

The distribution of this enrichment score was used to categorize sequences as "strongly enriching" or "weakly enriching" with a Z-score cutoff of 1.

4.9 | Motif analysis and sequence logos

A padding corresponding to the non-proteomic linker sequences within the surface display construct was appended to the N- ("xxxxxxialr") and C- ("riarxxxxxx") terminal of each 36-mer. Matches to the core Homer motif were identified in sequences from the T7-Pep library using the regular expression [PAILV]P..[FWY]. Motifs within two residues of the N-terminal linker were excluded from analysis due to the potential for artificial affinity boosts from the leucine present in the linker (Li et al., 2019). Sequences were aligned by the motif with both an N- and C-terminal flank of 10 residues. Position-specific scoring matrices (PSSMs) were generated using the publicly available software pLogo, with matches to the motif in all three populations (strongly enriching, weakly enriching, and non-enriching) serving as the background (O'Shea et al., 2013). PSSMs for sequences derived from the proteomic SPOT array were similarly aligned by the Homer motif. Final logos were generated from these PSSMs using the Logomaker Python library (Tareen and Kinney, 2020).

4.10 | BLI assay

BLI experiments were carried out on an Octet Red96 instrument (ForteBio). All assay steps were carried out in a 1:1 mixture of EVH1 gel filtration buffer (20 mM HEPES pH 7.6, 150 mM NaCl, 1 mM DTT) and PBS buffer (1× PBS pH 7.6, 1 mM DTT, 1% BSA, 0.1% Tween-20). Data were collected at room temperature using a shake speed of 1000 rpm at the default sampling rate. Streptavidin-coated tips (ForteBio) were equilibrated in the above buffer for 10 min. Biotinylated SUMO-peptides were loaded on the streptavidin tips to a target optical density between 0.5 and 1 nm and subsequently washed in the buffer for 60 s. The loaded tips were immersed in a solution of EVH1 domain to collect association data for 100 s. Subsequently, EVH1-bound tips were transferred to a well containing buffer, and dissociation data was collected for 100 s. This process was done iteratively, using the same tip, with increasing concentrations of EVH1 domain, for a total of eight concentrations.

Due to the fast kinetics of these interactions, we calculated K_D values using the equilibrium signal of the association step at each concentration of the EVH1 domain. We note that the binding phase associated with *cis-trans* proline isomerization observed by Greenwood is slow on the timescale of our measurements, and to the extent this applies to the ligands we studied here, we are measuring binding primarily to the population of peptide with appropriate proline conformations in the unbound state (Greenwood et al., 2014). At peptide concentrations below the K_D, the analysis below is not sensitive to this value. This signal was calculated as the average signal over the final 10 s of association, minus the average of the final 10 s of the dissociation step. The association data of a SUMO-only control was subtracted from that of the SUMO-peptides. The binding curve was fit and K_D value was extracted in Kaleidagraph using nonlinear least-squares fitting to the following equation:

$$y = \frac{C[\mathrm{EVH1}]}{K_D + [\mathrm{EVH1}]},$$

where y is the signal and C is the maximum signal at saturation. K_D values and their respective errors are reported as the average and standard deviation on three technical replicates.

Fold change error in Figure 4c was calculated by error propagation using the formula:

$$\sqrt{\left(\frac{SD_a}{\mu_a}\right)^2 + \left(\frac{SD_b}{\mu_b}\right)^2}.$$

4.11 | Proteome bioinformatic analysis

Bioinformatic analysis of the human (UP000005640; Organism 9606) and *D. discoideum* (UP000002195; Organism 44689) proteomes was performed using the one protein per gene datasets available on UniProt. Regions were classified as disordered using IUPred (Mészáros et al., 2018). Human orthologs for *D. discoideum* proteins were identified using the publicly available InParanoiDB9 (Human: 9606; Dictyostelium 44689) (Persson and Sonnhammer, 2023).

4.12 | SPOT array

ABI3 substitution and overlapping motif SPOT arrays were synthesized at the MIT Biopolymer Facility using an Intavis SPOT synthesis peptide arrayer system. At the N-terminus, the 20-mer peptides were capped with a Gly-Ser linker and acetylated. The peptides were linked to the cellulose membrane by a C-terminal PEG spacer. For the overlapping motif array, because many of the peptide sequences contain additional Ena/VASP and Homer motifs, each peptide was also synthesized as a control where the internal proline tract was mutated to poly-glycine. Native Cys residues were mutated to Ala, and the sequence of each peptide is provided in Table S2. The protocol for blocking and probing the membrane was adapted from Frank and Dübel (2006). The membrane was hydrated in 100% ethanol, washed three times with TBS (50 mM Tris pH 7.0, 137 mM NaCl, 2.7 mM KCl, 1 mM DTT) and then blocked overnight in MBS (TBS

+0.2% Tween-20, 2% (w/v) dry milk) at room temperature. The following day, the array was washed in T-TBS (TBS + 0.05% Tween-20) and then incubated with the protein sample in MBS (+1 μM DTT) for 3 h at room temperature. All array experiments were carried out with streptavidin-Cy3 (Thermo Fisher) pre-tetramerized EVH1 at a final monomer concentration of 0.5 μM. The membrane was washed three times in T-TBS prior to scanning on a GE Amersham Imager 680. SPOT intensities were calculated using the ImageJ analysis software (Abràmoff et al., 2004). No background correction was performed. For the overlapping peptides, the final intensity was calculated as the difference between the intensity of the wild-type and motif knockout control. An intensity threshold of 1000 was used to classify a peptide as having bound, with peptides that exhibited an intensity >1000 for only one domain being annotated as selective. Overlapping motifs that bound to both ENAH and Homer1 via SPOT array were assessed as candidate binding partners based on localization (gTEX/UniProt subcellular localization), interaction (HURI/BioGRID), and GO term data (Figure S3 in Data S1) (Lonsdale et al., 2013; Luck et al., 2020; Stark et al., 2006). GO term analysis was performed using the SLiMSearch 4 "shared functional annotations" tool (Krystkowiak and Davey, 2017). A *p*-value threshold of 0.001 for any paralogous Ena/VASP or Homer family member was used as a cutoff for marking GO terms as being shared.

AUTHOR CONTRIBUTIONS

Avinoam Singer: Conceptualization; data curation; formal analysis; writing – original draft; writing – review and editing. **Alejandra Ramos:** Data curation. **Amy E. Keating:** Conceptualization; funding acquisition; writing – original draft; writing – review and editing; supervision.

ACKNOWLEDGMENTS

We thank the Koch Institute's Robert A. Swanson (1969) Biotechnology Center for peptide array synthesis and flow cytometry expertise and services. We would also like to thank the MIT Biophysical Instrumentation Facility for access to BLI instrumentation. Lastly, we would like to thank the following individuals for helpful discussions: Sebastian Swanson, Jackson Halpin, Theresa Hwang, Dia Ghose, Jennifer Kosmatka, and Foster Birnbaum. A special thank you to Robert T. Sauer and Joseph Davis for their instrumental feedback throughout the course of this work.

FUNDING INFORMATION

Research reported in this publication was supported by the National Institute of General Medical Sciences of the National Institutes of Health under R01 GM129007 and R35 GM149227 to Amy E. Keating and National Cancer Institute Cancer Center (Core) Support Grant (CCSG) P30-CA14051. Avinoam Singer received support from National Institute of General Medical Sciences training award T32 GM007287. The content herein is solely the responsibility of the authors and does not represent the official views of any of the funding organizations.

ORCID

Avinoam Singer https://orcid.org/0009-0005-8736-9998
Amy E. Keating https://orcid.org/0000-0003-4074-8980

REFERENCES

Abràmoff MD, Magalhães PJ, Ram SJ. Image processing with imageJ. Biophoton Int. 2004;11(7):36–41. https://doi.org/10.1201/9781420005615.ax4

Acevedo LA, Greenwood AI, Nicholson LK. A noncanonical binding site in the EVH1 domain of vasodilator-stimulated phosphoprotein regulates its interactions with the proline rich region of zyxin. Biochemistry. 2017;56(35):4626–36. https://doi.org/10.1021/acs.biochem.7b00618

Ayala FJ, Rzhetsky A, Ayala FJ. Origin of the metazoan phyla: molecular clocks confirm paleontological estimates. Proc Natl Acad Sci USA. 1998;95(2):606–11. https://doi.org/10.1073/pnas.95.2.606

Bachmann C, Fischer L, Walter U, Reinhard M. The EVH2 domain of the vasodilator-stimulated phosphoprotein mediates tetramerization, F-Actin binding, and Actin bundle formation. J Biol Chem. 1999;274(33):23549–57. https://doi.org/10.1074/jbc.274.33.23549

Bae J, Sung BH, Cho IH, Kim SM, Song WK. Nesh regulates dendritic spine morphology and synapse formation. PLoS One. 2012;7(4):e34677. https://doi.org/10.1371/journal.pone.0034677

Ball LJ, Kühne R, Hoffmann B, Häfner A, Schmieder P, Volkmer-Engert R, et al. Dual epitope recognition by the VASP EVH1 domain modulates polyproline ligand specificity and binding affinity. EMBO J. 2000;19(18):4903–14. https://doi.org/10.1093/emboj/19.18.4903

Ball LJ, Kühne R, Schneider-Mergener J, Oschkinat H. Recognition of proline-rich motifs by protein-protein-interaction domains. Angew Chem Int Ed. 2005;44(19):2852–69. https://doi.org/10.1002/anie.200400618

Barzik M, Carl UD, Schubert WD, Frank R, Wehland J, Heinz DW. The N-terminal domain of Homer/Vesl is a new class II EVH1 domain. J Mol Biol. 2001;309(1):155–69. https://doi.org/10.1006/jmbi.2001.4640

Bear JE, Gertler FB. Ena/VASP: towards resolving a pointed controversy at the barbed end. J Cell Sci. 2009;122(12):1947–53. https://doi.org/10.1242/jcs.038125

Beneken J, Tu JC, Xiao B, Nuriya M, Yuan JP, Worley PF, et al. Structure of the Homer EVH1 domain-peptide complex reveals a new twist in polyproline recognition. Neuron. 2000;26:143–54. https://doi.org/10.1016/S0896-6273(00)81145-9

Bhattacharyya RP, Reményi A, Yeh BJ, Lim WA. Domains, motifs, and scaffolds: the role of modular interactions in the evolution and wiring of cell signaling circuits. Annu Rev Biochem. 2006;75:655–80. https://doi.org/10.1146/annurev.biochem.75.103004.142710

Brakeman PR, Lanahan AA, O'Brien R, Roche K, Barnes CA, Huganir RL, et al. Homer: a protein that selectively binds metabotropic glutamate receptors. Nature. 1997;386:284–8. https://doi.org/10.1038/386284a0

Bugge K, Brakti I, Fernandes CB, Dreier JE, Lundsgaard JE, Olsen JG, et al. Interactions by disorder – a matter of context. Front Mol Biosci. 2020;7(June):1–16. https://doi.org/10.3389/fmolb.2020.00110

Burkhardt P, Grønborg M, McDonald K, Sulur T, Wang Q, King N. Evolutionary insights into premetazoan functions of the neuronal protein Homer. Mol Biol Evol. 2014;31:2342–55. https://doi.org/10.1093/molbev/msu178

Bushnell B, Rood J, Singer E. BBMerge – accurate paired shotgun read merging via overlap. PLoS One. 2017;12(10):1–15. https://doi.org/10.1371/journal.pone.0185056

Cesareni G, Panni S, Nardelli G, Castagnoli L. Can we infer peptide recognition specificity mediated by SH3 domains? FEBS Lett. 2002;513(1):38–44. https://doi.org/10.1016/S0014-5793(01)03307-5

Chen S, Zhang Y, Wang H, Zeng YY, Li Z, Li ML, et al. WW domain-binding protein 2 acts as an oncogene by modulating the activity of the glycolytic enzyme ENO1 in glioma article. Cell Death Dis. 2018;9(3):347. https://doi.org/10.1038/s41419-018-0376-5

Chen XJ, Squarr AJ, Stephan R, Chen B, Higgins TE, Barry DJ, et al. Ena/VASP proteins cooperate with the WAVE complex to regulate the actin cytoskeleton. Dev Cell. 2014;30(5):569–84. https://doi.org/10.1016/j.devcel.2014.08.001

Clifton NE, Trent S, Thomas KL, Hall J. Regulation and function of activity-dependent Homer in synaptic plasticity. Mol Neuropsychiatry. 2019;5(3):147–61. https://doi.org/10.1159/000500267

Conant GC, Wolfe KH. Turning a hobby into a job: how duplicated genes find new functions. Nat Rev Genet. 2008;9(12):938–50. https://doi.org/10.1038/nrg2482

Davey NE, Van Roey K, Weatheritt RJ, Toedt G, Uyar B, Altenberg B, et al. Attributes of short linear motifs. Mol BioSyst. 2012;8(1):268–81. https://doi.org/10.1039/c1mb05231d

Davey NE, Cyert MS, Moses AM. Short linear motifs – ex nihilo evolution of protein regulation. Cell Commun Signal. 2015;13:43. https://doi.org/10.1186/s12964-015-0120-z

Davey NE, Seo MH, Yadav VK, Jeon J, Nim S, Krystkowiak I, et al. Discovery of short linear motif-mediated interactions through phage display of intrinsically disordered regions of the human proteome. FEBS J. 2017;284(3):485–98. https://doi.org/10.1111/febs.13995

Dinkel H, Michael S, Weatheritt RJ, Davey NE, Van Roey K, Altenberg B, et al. ELM – the database of eukaryotic linear motifs. Nucleic Acids Res. 2012;40(D1):242–51. https://doi.org/10.1093/nar/gkr1064

Drees F, Gertler FB. Ena/VASP: proteins at the tip of the nervous system. Curr Opin Neurobiol. 2008;18(1):53–9. https://doi.org/10.1016/j.conb.2008.05.007

Faix J, Rottner K. Ena/VASP proteins in cell edge protrusion, migration and adhesion. J Cell Sci. 2022;135(6):jcs259226. https://doi.org/10.1242/jcs.259226

Foight GW, Keating AE. Comparison of the peptide binding preferences of three closely related TRAF paralogs: TRAF2, TRAF3, and TRAF5. Protein Sci. 2016;25:1273–89. https://doi.org/10.1002/pro.2881

Frank R, Dübel S. Analysis of protein interactions with immobilized peptide arrays synthesized on membrane supports. Cold Spring Harb Protoc. 2006;2006(4):pdb.prot4566. https://doi.org/10.1101/pdb.prot4566

Fraser HB, Hirsh AE, Steinmetz LM, Scharfe C, Feldman MW. Evolutionary rate in the protein interaction network. Science. 2002;296(5568):750–2. https://doi.org/10.1126/science.1068696

Fraser HB, Wall DP, Hirsh AE. A simple dependence between protein evolution rate and the number of protein-protein interactions. BMC Evol Biol. 2003;6:6–11.

Ghose DA, Przydzial KE, Mahoney EM, Keating AELM. Marginal specificity in protein interactions constrains evolution of a paralogous family. Proc Natl Acad Sci. 2023;120(18):e2221163120. https://doi.org/10.1073/pnas

Goulding SP, Szumlinski KK, Contet C, MacCoss MJ, Wu CC. A mass spectrometry-based proteomic analysis of Homer2-interacting proteins in the mouse brain. J Proteome. 2017;166:127–37. https://doi.org/10.1016/j.jprot.2017.07.008

Greenwood AI, Kwon J, Nicholson LK. Isomerase-catalyzed binding of interleukin-1 receptor-associated kinase 1 to the EVH1 domain of vasodilator-stimulated phosphoprotein. Biochemistry. 2014;53(22):3593–607. https://doi.org/10.1021/bi500031e

Hahn MW, Kern AD. Comparative genomics of centrality and essentiality in three eukaryotic protein-interaction networks. Mol Biol Evol. 2005;22(4):803–6. https://doi.org/10.1093/molbev/msi072

Han YH, Chung CY, Wessels D, Stephens S, Titus MA, Soll DR, et al. Requirement of a vasodilator-stimulated phosphoprotein family member for cell adhesion, the formation of filopodia, and chemotaxis in dictyostelium. J Biol Chem. 2002;277(51):49877–87. https://doi.org/10.1074/jbc.M209107200

Hornbeck PV, Kornhauser JM, Tkachev S, Zhang B, Skrzypek E, Murray B, et al. PhosphoSitePlus: a comprehensive resource for investigating the structure and function of experimentally determined post-translational modifications in man and mouse. Nucleic Acids Res. 2012;40(D1):261–70. https://doi.org/10.1093/nar/gkr1122

Huang GN, Huso DL, Bouyain S, Tu J, McCorkell KA, May MJ, et al. NFAT binding and regulation of T cell activation by the cytoplasmic scaffolding homer proteins. Science. 2008;319(5862):476–81. https://doi.org/10.1126/science.1151227

Hüttelmaier S, Harbeck B, Steffens NO, Meßerschmidt T, Illenberger S, Jockusch BM. Characterization of the actin binding properties of the vasodilator-stimulated phosphoprotein VASP. FEBS Lett. 1999;451(1):68–74. https://doi.org/10.1016/S0014-5793(99)00546-3

Hwang T, Parker SS, Hill SM, Ilunga MW, Grant RA, Mouneimne G, et al. A distributed residue network permits conformational binding specificity in a conserved family of actin remodelers. elife. 2021;10:1–21. https://doi.org/10.7554/eLife.70601

Hwang T, Parker SS, Hill SM, Grant RA, Ilunga MW, Sivaraman V, et al. Native proline-rich motifs exploit sequence context to target actin-remodeling Ena/VASP protein ENAH. elife. 2022;11:1–21. https://doi.org/10.7554/eLife.70680

Jumper J, Evans R, Pritzel A, Green T, Figurnov M, Ronneberger O, et al. Highly accurate protein structure prediction with AlphaFold. Nature. 2021;596(7873):583–9. https://doi.org/10.1038/s41586-021-03819-2

Körber S, Faix J. VASP boosts protrusive activity of macroendocytic cups and drives phagosome rocketing after internalization. Eur J Cell Biol. 2022;101(2):151200. https://doi.org/10.1016/j.ejcb.2022.151200

Krystkowiak I, Davey NE. SLiMSearch: a framework for proteome-wide discovery and annotation of functional modules in intrinsically disordered regions. Nucleic Acids Res. 2017;45(W1):W464–9. https://doi.org/10.1093/nar/gkx238

La Torre A, Del Mar Masdeu M, Cotrufo T, Moubarak RS, del Río JA, Comella JX, et al. A role for the tyrosine kinase ACK1 in neurotrophin signaling and neuronal extension and branching. Cell Death Dis. 2013;4(4):1–14. https://doi.org/10.1038/cddis.2013.99

Landgraf C, Panni S, Montecchi-Palazzi L, Castagnoli L, Schneider-Mergener J, Volkmer-Engert R, et al. Protein interaction networks by proteome peptide scanning. PLoS Biol. 2004;2(1):94–103. https://doi.org/10.1371/journal.pbio.0020014

Lanier LM, Gates MA, Witke W, Menzies AS, Wehman AM, Macklis JD, et al. Mena is required for neurulation and commissure formation. Neuron. 1999;22(2):313–25. https://doi.org/10.1016/S0896-6273(00)81092-2

Larman HB, Zhao Z, Laserson U, Li MZ, Ciccia A, Gakidis MAM, et al. Autoantigen discovery with a synthetic human peptidome. Nat Biotechnol. 2011;29(6):535–41. https://doi.org/10.1038/nbt.1856

Li J, Zhu R, Chen K, Zheng H, Zhao H, Yuan C, et al. Potent and specific Atg8-targeting autophagy inhibitory peptides from giant ankyrins. Nat Chem Biol. 2018;14(8):778–87. https://doi.org/10.1038/s41589-018-0082-8

Li W, Godzik A. Cd-hit: a fast program for clustering and comparing large sets of protein or nucleotide sequences. Bioinformatics. 2006;22(13):1658–9. https://doi.org/10.1093/bioinformatics/btl158

Li Z, Liu H, Li J, Yang Q, Feng Z, Li Y, et al. Homer tetramer promotes actin bundling activity of Drebrin. Structure. 2019;27(1):27–38.e4. https://doi.org/10.1016/j.str.2018.10.011

Litschko C, Linkner J, Brühmann S, Stradal TEB, Reinl T, Jänsch L, et al. Differential functions of WAVE regulatory complex subunits in the regulation of actin-driven processes. Eur J Cell Biol. 2017;96(8):715–27. https://doi.org/10.1016/j.ejcb.2017.08.003

Lonsdale J, Thomas J, Salvatore M, Phillips R, Lo E, Shad S, et al. The genotype-tissue expression (GTEx) project. Nat Genet. 2013;45(6):580–5. https://doi.org/10.1038/ng.2653

Luck K, Kim DK, Lambourne L, Spirohn K, Begg BE, Bian W, et al. A reference map of the human binary protein interactome. Nature. 2020;580(7803):402–8. https://doi.org/10.1038/s41586-020-2188-x

Makino T, Gojobori T. Evolution of protein-protein interaction network. Genome Dyn. 2007;3:13–29.

McClune CJ, Laub MT. Constraints on the expansion of paralogous protein families. Curr Biol. 2020;30(10):R460–4. https://doi.org/10.1016/j.cub.2020.02.075

McClune CJ, Alvarez-Buylla A, Voigt CA, Laub MT. Engineering orthogonal signalling pathways reveals the sparse occupancy of sequence space. Nature. 2019;574(7780):702–6. https://doi.org/10.1038/s41586-019-1639-8

Mészáros B, Erdös G, Dosztányi Z. IUPred2A: context-dependent prediction of protein disorder as a function of redox state and protein binding. Nucleic Acids Res. 2018;46:W329–37. https://doi.org/10.1093/nar/gky384

Mirdita M, Schütze K, Moriwaki Y, Heo L, Ovchinnikov S, Steinegger M. ColabFold: making protein folding accessible to all. Nat Methods. 2022;19(6):679–82. https://doi.org/10.1038/s41592-022-01488-1

Muranishi Y, Terada K, Furukawa T. An essential role for Rax in retina and neuroendocrine system development. Develop Growth Differ. 2012;54(3):341–8. https://doi.org/10.1111/j.1440-169X.2012.01337.x

Niebuhr K, Ebel F, Frank R, Reinhard M, Domann E, Carl UD, et al. A novel proline-rich motif present in ActA of Listeria monocytogenes and cytoskeletal proteins is the ligand for the EVH1 domain, a protein module present in the Ena/VASP family. EMBO J. 1997;16(17):5433–44. https://doi.org/10.1093/emboj/16.17.5433

Orlando LR, Ayala R, Kett LR, Curley AA, Duffner J, Bragg DC, et al. Phosphorylation of the homer-binding domain of group i metabotropic glutamate receptors by cyclin-dependent kinase 5. J Neurochem. 2009;110(2):557–69. https://doi.org/10.1111/j.1471-4159.2009.06139.x

O'Shea JP, Chou MF, Quader SA, Ryan JK, Church GM, Schwartz D. PLogo: a probabilistic approach to visualizing sequence motifs. Nat Methods. 2013;10(12):1211–2. https://doi.org/10.1038/nmeth.2646

Oxley CL, Anthis NJ, Lowe ED, Vakonakis I, Campbell ID, Wegener KL. An integrin phosphorylation switch: the effect of β3 integrin tail phosphorylation on Dok1 and talin binding. J Biol Chem. 2008;283(9):5420–6. https://doi.org/10.1074/jbc.M709435200

Persson E, Sonnhammer ELL. InParanoiDB 9: ortholog groups for protein domains and full-length proteins. J Mol Biol. 2023;435(14):168001. https://doi.org/10.1016/j.jmb.2023.168001

Peterson FC, Volkman BF. Diversity of polyproline recognition by EVH1 domains. Front Biosci (Landmark Ed). 2009;14:833–46. https://doi.org/10.2741/3281

Prehoda KE, Lee DJ, Lim WA. Structure of the enabled/VASP homology 1 domain-peptide complex: a key component in the spatial control of actin assembly. Cell. 1999;97(4):471–80. https://doi.org/10.1016/s0092-8674(00)80757-6

Reimer U, Scherer G, Drewello M, Kruber S, Schutkowski M, Fischer G. Side-chain effects on peptidyl-prolyl cis/trans isomerisation. J Mol Biol. 2014;29(2):399–424.

Reinhard M, Jouvenal K, Tripier D, Walter U. Identification, purification, and characterization of a zyxin-related protein that binds the focal adhesion and microfilament protein VASP (vasodilator-stimulated phosphoprotein). Proc Natl Acad Sci USA. 1995;92(17):7956–60. https://doi.org/10.1073/pnas.92.17.7956

Rice JJ, Daugherty PS. Directed evolution of a biterminal bacterial display scaffold enhances the display of diverse peptides. Protein Eng Des Sel. 2008;21(7):435–42. https://doi.org/10.1093/protein/gzn020

Rong R, Ahn JY, Huang H, Nagata E, Kalman D, Kapp JA, et al. PI3 kinase enhancer-Homer complex couples mGluRI to PI3 kinase, preventing neuronal apoptosis. Nat Neurosci. 2003;6(11):1153–61. https://doi.org/10.1038/nn1134

Rottner K, Behrendt B, Small JV, Wehland J. VASP dynamics during lamellipodia protrusion. Nat Cell Biol. 1999;1(5):321–2. https://doi.org/10.1038/13040

Rottner K, Stradal TEB, Chen B. WAVE regulatory complex. Curr Biol. 2021;31(10):R512–7. https://doi.org/10.1016/j.cub.2021.01.086

Sala C, Piëch V, Wilson N, Passafaro M, Liu G, Sheng M. Regulation of dendritic spine morphology and synaptic function by shank and Homer. Neuron. 2001;31(1):115–30. https://doi.org/10.1016/s0896-6273(01)00339-7

Schreiner D, Müller K, Hofer HW. The intracellular domain of the human protocadherin hFat1 interacts with Homer signalling scaffolding proteins. FEBS Lett. 2006;580(22):5295–300. https://doi.org/10.1016/j.febslet.2006.08.079

Shiraishi-Yamaguchi Y, Furuichi T. The Homer family proteins. Genome Biol. 2007;8(2):1–12. https://doi.org/10.1186/gb-2007-8-2-206

Soderling SH, Guire ES, Kaech S, White J, Zhang F, Schutz K, et al. A WAVE-1 and WRP signaling complex regulates spine density, synaptic plasticity, and memory. J Neurosci. 2007;27(2):355–65. https://doi.org/10.1523/JNEUROSCI.3209-06.2006

Stark C, Breitkreutz BJ, Reguly T, Boucher L, Breitkreutz A, Tyers M. BioGRID: a general repository for interaction datasets. Nucleic Acids Res. 2006;34(Database issue):D535–9. https://doi.org/10.1093/nar/gkj109

Stillman M, Lautz JD, Johnson RS, MacCoss MJ, Smith SEP. Activity dependent dissociation of the Homer1 interactome. Sci Rep. 2022;12(1):1–10. https://doi.org/10.1038/s41598-022-07179-3

Tareen A, Kinney JB. Logomaker: beautiful sequence logos in python. Bioinformatics. 2020;36(7):2272–4. https://doi.org/10.1093/bioinformatics/btz921

Tompa P, Davey NE, Gibson TJ, Babu MM. A million peptide motifs for the molecular biologist. Mol Cell. 2014;55(2):161–9. https://doi.org/10.1016/j.molcel.2014.05.032

Tu JC, Xiao B, Yuan JP, Lanahan AA, Leoffert K, Li M, et al. Homer binds a novel proline-rich motif and links group 1 metabotropic glutamate receptors with IP3 receptors. Neuron. 1998;21:717–26. https://ac.els-cdn.com/S0896627300805899/1-s2.0-S0896627300805899-main.pdf?_tid=bb2fc94d-09e7-4c3b-bc6b-377a479a6f8b&acdnat=1531297208_345d985e711b9c3d89b47b67acaee95d

Tu JC, Xiao B, Naisbitt S, Yuan JP, Petralia RS, Brakeman P, et al. Coupling of mGluR/Homer and PSD-95 complexes by the shank family of postsynaptic density proteins. Neuron. 1999;23(3):583–92. https://doi.org/10.1016/S0896-6273(00)80810-7

Ueki Y, Kruse T, Weisser MB, Sundell GN, Larsen MSY, Mendez BL, et al. A consensus binding motif for the PP4 protein phosphatase. Mol Cell. 2019;76(6):953–964.e6. https://doi.org/10.1016/j.molcel.2019.08.029

Urbanek A, Popovic M, Elena-Real CA, Morató A, Estaña A, Fournet A, et al. Evidence of the reduced abundance of proline cis conformation in protein poly proline tracts. J Am Chem Soc. 2020;142(17):7976–86. https://doi.org/10.1021/jacs.0c02263

Uyar B, Weatheritt RJ, Dinkel H, Davey NE, Gibson TJ. Proteome-wide analysis of human disease mutations in short linear motifs: neglected players in cancer? Mol BioSyst. 2014;10(10):2626–42. https://doi.org/10.1039/c4mb00290c

Van Roey K, Gibson TJ, Davey NE. Motif switches: decision-making in cell regulation. Curr Opin Struct Biol. 2012;22(3):378–85. https://doi.org/10.1016/j.sbi.2012.03.004

Van Roey K, Dinkel H, Weatheritt RJ, Gibson TJ, Davey NE. The switches.ELM resource: a compendium of conditional regulatory interaction interfaces. Sci Signal. 2013;6(269):1–11. https://doi.org/10.1126/scisignal.2003345

Van Roey K, Uyar B, Weatheritt RJ, Dinkel H, Seiler M, Budd A, et al. Short linear motifs: ubiquitous and functionally diverse protein interaction modules directing cell regulation. Chem Rev. 2014;114(13):6733–78. https://doi.org/10.1021/cr400585q

Vogel C, Chothia C. Protein family expansions and biological complexity. PLoS Comput Biol. 2006;2(5):370–82. https://doi.org/10.1371/journal.pcbi.0020048

Wright PE, Dyson HJ. Intrinsically disordered proteins in cellular signalling and regulation. Nat Rev Mol Cell Biol. 2015;16(1):18–29. https://doi.org/10.1038/nrm3920

Wu J, Pipathsouk A, Keizer-Gunnink A, Fusetti F, Alkema W, Liu S, et al. Homer3 regulates the establishment of neutrophil polarity. Mol Biol Cell. 2015;26:1629–39. https://doi.org/10.1091/mbc.E14-07-1197

Xiao B, Tu JC, Petralia RS, Yuan JP, Doan A, Breder CD, et al. Homer regulates the association of group 1 metabotropic glutamate receptors with multivalent complexes of Homer-related, synaptic proteins. Neuron. 1998;21(4):707–16. https://doi.org/10.1016/S0896-6273(00)80588-7

Yoon S, Piguel NH, Khalatyan N, Dionisio LE, Savas JN, Penzes P. Homer1 promotes dendritic spine growth through ankyrin-G and its loss reshapes the synaptic proteome. Mol Psychiatry. 2021;26:1775–89. https://doi.org/10.1038/s41380-020-00991-1

Yuan JP, Kiselyov K, Shin DM, Chen J, Shcheynikov N, Kang SH, et al. Homer binds TRPC family channels and is required for gating of TRPC1 by IP3 receptors. Cell. 2003;114(6):777–89. https://doi.org/10.1016/S0092-8674(03)00716-5

Zarrinpar A, Park SH, Lim WA. Optimization of specificity in a cellular protein interaction network by negative selection. Nature. 2003;426(6967):676–80. https://doi.org/10.1038/nature02178

Zhang J, Chen T, Mao Q, Lin J, Jia J, Li S, et al. PDGFR-β-activated ACK1-AKT signaling promotes glioma tumorigenesis. Int J Cancer. 2015;136(8):1769–80. https://doi.org/10.1002/ijc.29234

Zondlo NJ. Aromatic-proline interactions: electronically tunable CH/π interactions. Acc Chem Res. 2013;46(4):1039–49.

SUPPORTING INFORMATION

Additional supporting information can be found online in the Supporting Information section at the end of this article.

How to cite this article: Singer A, Ramos A, Keating AE. Elaboration of the Homer1 recognition landscape reveals incomplete divergence of paralogous EVH1 domains. Protein Science. 2024;33(8):e5094. https://doi.org/10.1002/pro.5094